Giant, 15, 2023, 100170

Full-length article

Construction Archimedean tiling patterns based on soft materials from block copolymers and covalent organic frameworks

Shiao-Wei Kuo

Department of Materials and Optoelectronic Science, Center of Crystal Research, National Sun Yat-Sen University, Kaohsiung 804, Taiwan

Keywords: **Archimedean tiling patterns, Covalent organic frameworks, Block copolymers, Self-assembled structures and Frank-Kasper phase**

Soft materials based on block copolymers or covalent organic frameworks (COFs) that exhibit Archimedean tiling patterns have attracted significant interest due to their potential applications in nanopatterning, nanocomposites, and shape selectivity. Additionally, researchers have widely investigated the corresponding microporous or mesoporous materials with Archimedean tiling from COF or block copolymers as templates with high surface area and pore volume, or tunable porosity with different length scales, in separation, energy storage, drug delivery, photo-catalysis, photovoltaic solar cells, and chemical sensing. This review article highlights recent progress in constructing Archimedean tiling patterns based on the creation of ordered structures from block copolymers by self-assembly and the direct synthesis of COF materials with various topologies.

1 Introduction

Because of the experimental finding the two-dimensional (2D) graphene materials [1,2], the synthesis of new 2D materials has become a hot field in recent years such as metal organic frameworks (MOF) [3–5], covalent organic frameworks (COF) [6–10], transition metal-dichalcogenides [11,12], borophene [13,14] and others [15]. In general, the periodic arrangements in a plane are large and could be constructed for simple class of 2D materials. For example, the class of lattices produced by taking into account one site in each vertex of the **k**-uniform titling of the plane. The simplest lattice is given by $\mathbf{k} = 1$, where **k** represents the number of non-equivalent vertexes, indicating only one non-equivalent vertex (also called uniform tiling) as Archimedean titling [16–18].

Fig. 1 illustrates 11 different Archimedean tiling patterns, which are non-periodic and do not repeat in the exact same way [19–24]. These patterns are classified using the notation of Archimedean tiling, which lists the types of polygons forming each vertex and the number of times they appear. For instance, triangular tiling (3^6) denotes that 6 equilateral triangles (each with an internal angle of 60°) occupy 360° at a point. Square tiling (4^4) corresponds to 4 squares (each with an internal angle of 90°) around each vertex, and hexagonal tiling (6^3) consists of 3 hexagons (each with an internal angle of 120°) making up 360° at a point. These 3 patterns are known as regular Archimedean tilings of the plane because they feature only one shape, such as a triangle, square, or hexagon, in each tiling.

The remaining 8 tiling patterns in Fig. 1 belong to the category of semiregular Archimedean tiling as each tiling involves more than two types of shapes [19–24]. The snub hexagonal tiling

E-mail address: kuosw@faculty.nsysu.edu.tw
Received 12 April 2023; Received in revised form 16 May 2023; Accepted 20 May 2023

https://doi.org/10.1016/j.giant.2023.100170

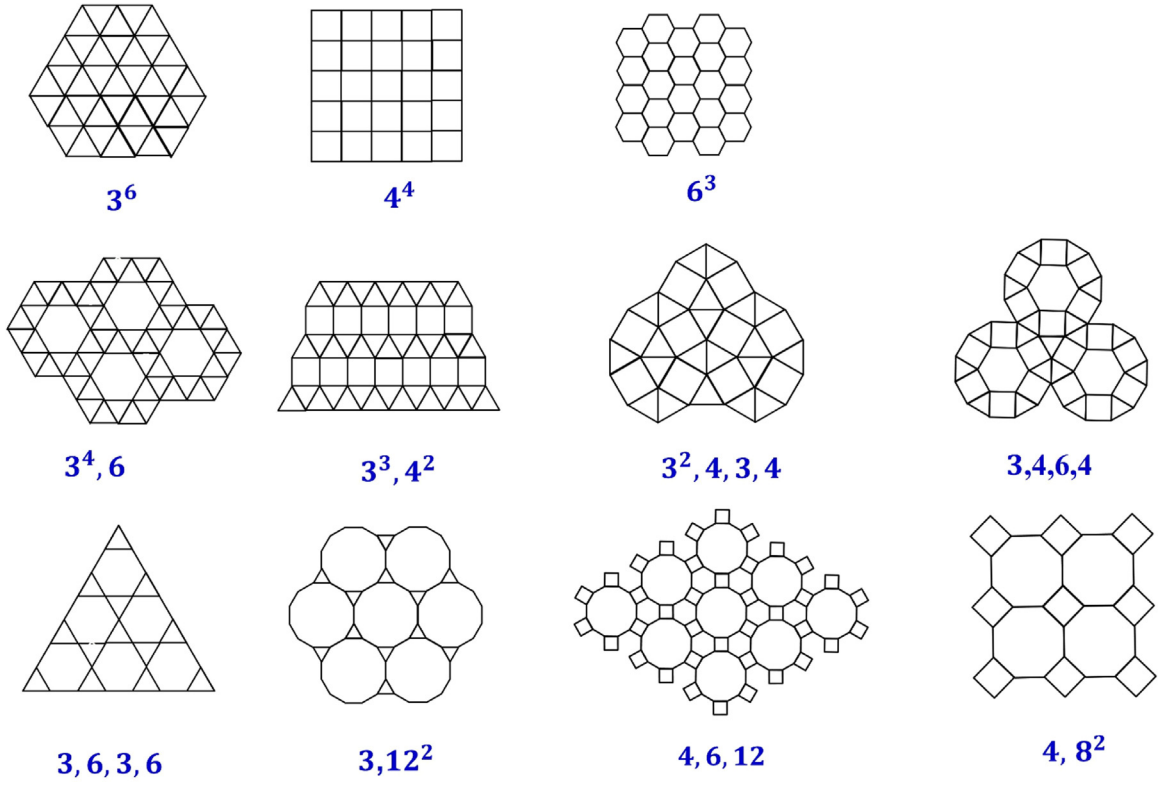

Fig. 1

The common characteristic of the eleven Archimedean tiling patterns that all involve tessellating regular polygons in such a way that all vertices have the same arrangement or environment [19–24].

(3^4,6) consists of 4 triangles and one hexagon at each vertex. The elongated triangular tiling (3^3,4^2) has 3 triangles and 2 squares on each vertex. The snub square tiling (3^2,4,3,4) has a sequence of 2 triangles, 1 square, 1 triangle, and 1 square at each vertex. The rhombitrihexagonal tiling (3,4,6,4) contains 1 triangle, 2 squares, and 1 hexagon at each vertex. The trihexagonal tiling (3,6,3,6), also assigned as the Kagome lattice due to its use in Japanese basketry, features 2 triangles and 2 hexagons alternating around each vertex. The truncated hexagonal tiling (3,12^2) has 1 triangle and 2 dodecagons on each vertex. The truncated trihexagonal tiling (4,6,12) includes 1 square, 1 hexagon, and 1 dodecagon around each vertex. The truncated square tiling (4,8^2) has 1 square and 2 octagons on each vertex. Each Archimedean tiling has unique characteristics and properties that have been extensively studied by mathematicians and material scientists due to their mathematical complexity and aesthetically pleasing shapes.

Archimedean tiling patterns have been observed not only in highly ordered metal alloys [25,26], but also in self-assembled structures from soft materials such as surfactants [27], block copolymers [19–23,28,29], liquid crystals [30], and giant amphiphiles [31–35]. In addition to self-assembled structures, the direct synthesize Archimedean tiling patterns have also been able to synthesize various topologies from COFs by controlling the geometry and dimensions of the building monomers in recent years. The typical topologies of COFs can be assigned as regular Archimedean tiling, including (3^6), (4^4), and (6^3) of the plane, but there has also been much recent interest in constructing new COF materials with semiregular Archimedean tiling patterns [36]. This review emphasis on the recent progress in the preparation of soft materials with Archimedean tiling patterns based on block copolymers and COFs.

2 Archimedean tiling patterns based on block copolymers

Self-assembled nanostructures from diblock copolymers exhibit typical structures such as lamellae, double gyroid, spherical, and hexagonal packed cylinder structures in the bulk state, as shown in Fig. 2(a) [37]. These structures are moderately simple and cost-effective to make large-scale nano-patterns. The driving force behind the formation of these structures is the microphase separation mechanism that results from the attractive interaction between the covalent bond linkage and the repulsive interaction as a result of the immiscibility of the block copolymer segments, as exhibited in Fig. 2(b) [34]. The formation of these structures is primarily dependent on the volume fraction, degree of polymerization (N), and interaction parameter (χ) [38,39].

Besides diblock copolymers, ABC linear triblock copolymers have also been widely explored, and various self-assembled structures have been found, such as three-phase lamellae, core-shell cylinders, and other complicated structures [40,41]. However, the ability to create novel self-assembled structures is limited by the typical chain connectivity parameters present in ABC linear triblock copolymers.

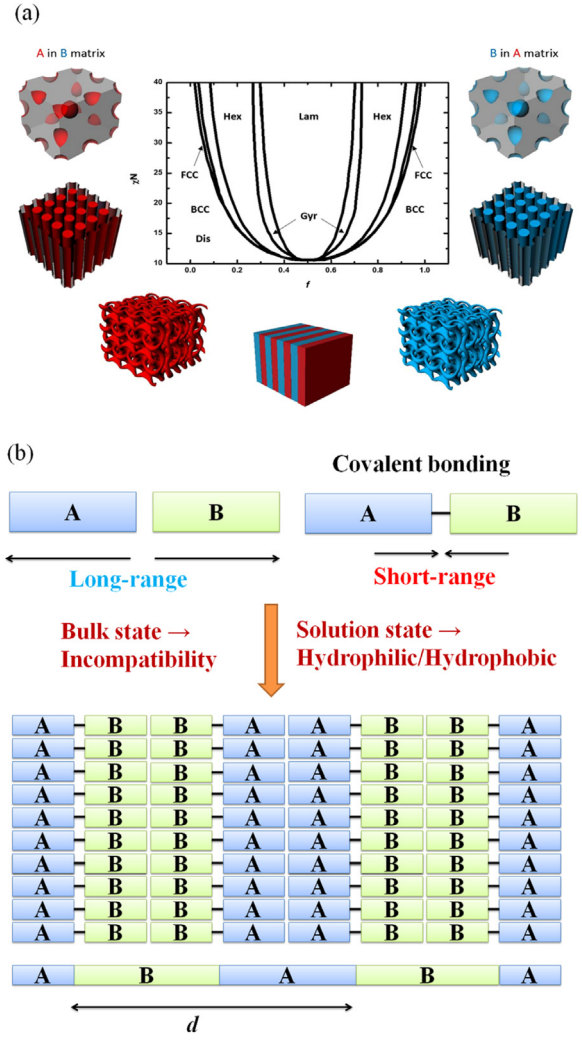

Fig. 2

(a) A typical phase diagram in a bulk state for the diblock copolymer as a function of temperature and composition and (b) diblock copolymers experience long-range repulsive interactions due to the incompatibility of the different blocks and short-range attractive interactions due to the covalent bond [37].

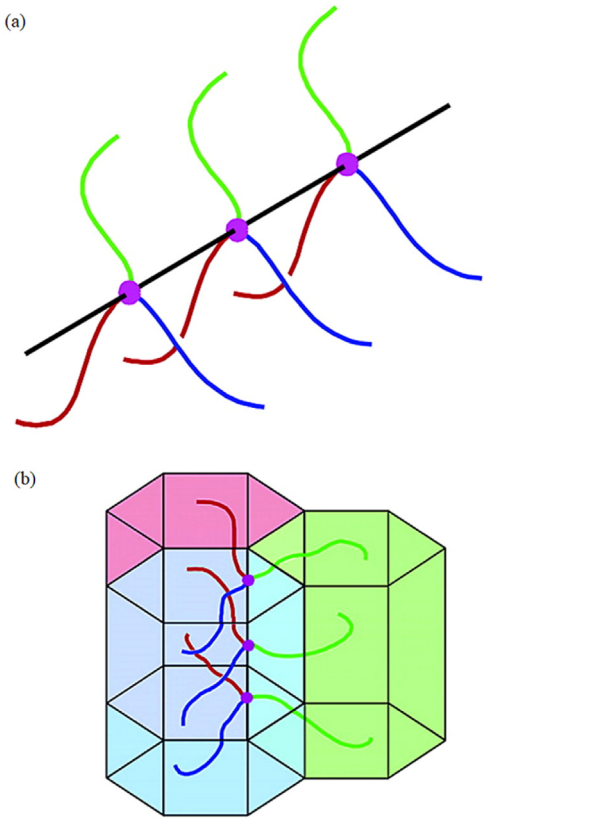

Fig. 3

(a) In 1D junction point alignment, a series of nodes are linearly arranged with each node representing the intersection of three polymer chains and (b) the self-assembly process of ABC star triblock copolymer involves the creation of cylindrical structures composed of alternating layers of the A, B, and C blocks. (Adapted from Ref. [22] with permission; copyright 2007, American Chemical Society).

In contrast, the self-assembled structures from ABC star triblock copolymers are completely different from those of ABC linear triblock copolymers due to the geometrical constraint of their junction points [23,42–46]. The junction points of ABC star triblock copolymers were constricted to a line in the strong segregation regime, where three interfaces meet together. These polymers tend to present 2D Archimedean tiling patterns since the interfaces of each polymer segment could be flat because of the repulsive force of unconnected branches, as shown in Fig. 3 [22].

Abetz et al. and Takano et al. have proposed on the preparation of various Archimedean tiling patterns using star triblock copolymers [44,47]. Abetz et al. utilized PS-*b*-PB-*b*-P2VP star triblock copolymer to produce (4,6,12) and (4,8^2) tiling patterns [47]. On the other hand, Takano et al. synthesized PI-*b*-PS-*b*-P2VP$_x$ star triblock copolymers with varying volume ratios of P2VP segment and demonstrated different Archimedean tiling patterns. These included (6^3) for $x = 0.7$ (Fig. 4(a)), (4,8^2) for $x = 1.2$ (Fig. 4(b)), (3^2,4,3,4) for $x = 1.3$ (Fig. 4(c)), and (4,6,12) for $x = 1.9$ (Fig. 4(d)) [48].

Another PI-*b*-PS-*b*-P2VP star triblock copolymer with various volume ratios of PS segment by blending with PS and PI homopolymers as PI$_{1.0}$-b-PS$_y$-b-P2VP$_{2.0}$ also exhibited several Archimedean tiling patterns, such as (4,6,12) for $y = 1.3$ (Fig. 5(a)), (3,4,6,4) for $y = 1.8$ (Fig. 5(b)), (3^2,4,3,4) for $y = 2.3$ (Fig. 5(c)), and (4,8^2) for $y = 2.7$ (Fig. 5(d)) [22,43].

The micro-beam 2D SAXS pattern of PI$_{1.0}$-*b*-PS$_{1.8}$-*b*-P2VP$_{2.0}$ was shown in Fig. 6(a), featuring 12 diffraction spots at lower q values, with 8 spots belonging to {21} and the other 4 to {20}. The corresponding TEM image was shown in Fig. 6(b), revealing the (3^2,4,3,4) tiling pattern. The TEM image of PI$_{1.0}$-*b*-PS$_{2.3}$-*b*-P2VP$_{2.0}$ sample was displayed in Fig. 6(c), and its corresponding micro-beam 2D SAXS pattern was shown in Fig. 6(d), exhibiting a 12-fold symmetry nature with (3^2,4,3,4) tiling pattern [22].

As mentioned in Fig. 5, it shows that blending homopolymers or diblock copolymers with diblock (AB) or triblock (ABC) copolymers can be used to adjust the volume fraction of each block segment and promote the formation of well-defined self-assembled or Archimedean tiling structures through hydrogen

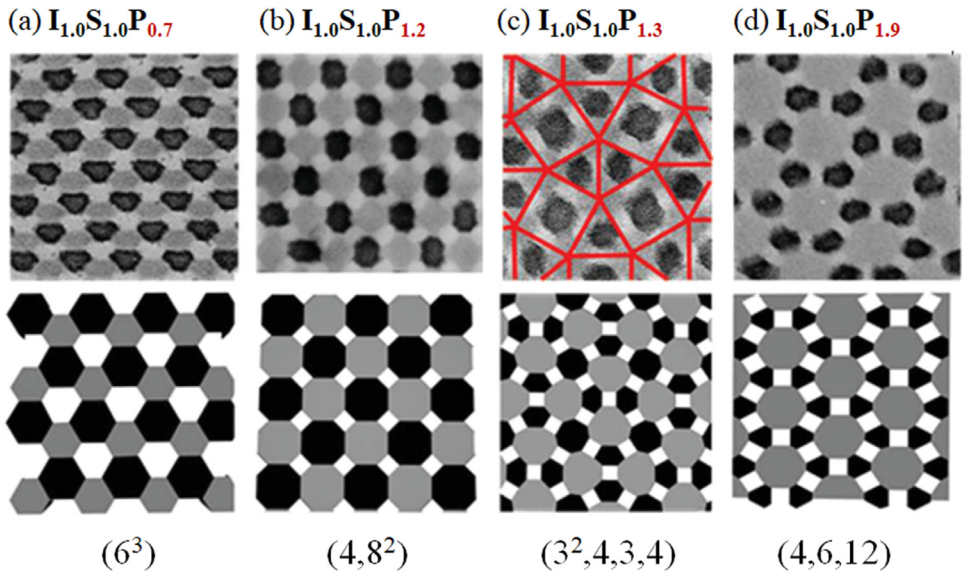

Fig. 4

The $I_{1.0}S_{1.0}P_x$ type of star triblock copolymers fearing four distinct types of Archimedean tilings, which can be represented by (a) (6^3), (b) $(4,8^2)$, (c) $(3^2,4,3,4)$, and (d) (4,6,12). The corresponding tilings are shown in TEM images are at the top of figures, while their schematics are depicted at the bottom. (Adapted from Ref. [48] with permission; copyright 2020, American Chemical Society).

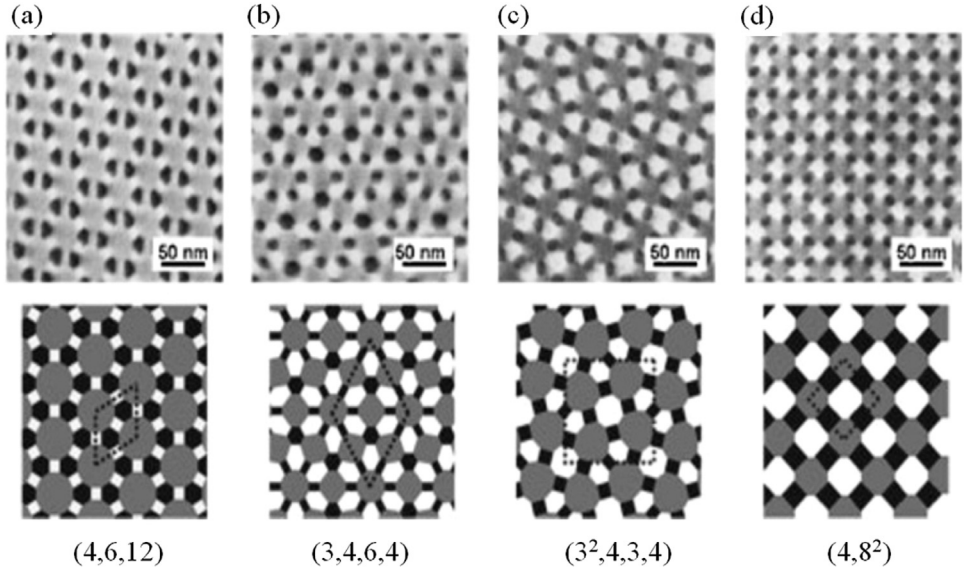

Fig. 5

The $PI_{1.0}$-b-PS_y-b-$P2VP_{2.0}$ type of star triblock copolymers fearing four distinct types of Archimedean tilings, which can be represented by (4,6,12), (3,4,6,4), $(3^2,4,3,4)$, and $(4,8^2)$. The corresponding tilings are shown in TEM images are at the top of figures, while their schematics are depicted at the bottom. (Adapted from Ref. [43] with permission; copyright 2006, American Chemical Society).

bonding interactions. For instance, Kim et al. employed a PS-*b*-PVPh and blended it with other highly asymmetric PS-*b*-P4VP or PS-*b*-P2VP diblock copolymers with a strong hydrogen bonding interaction between PVPh/P2VP or PVPh/P4VP (B/C) binary pairs. They observed an unusual highly asymmetric lamellar structure that contained a high volume fraction (80 vol.%) of the PS segment, which is not commonly observed for typical diblock copolymers [49].

In addition to blending homopolymers or diblock copolymers with diblock or triblock copolymers, another approach to prepare complex [50–58] or hierarchical structures is through blending AB with CD diblock copolymers using hydrogen bonding interactions [22,59–64]. This method can also be applied to the synthesis of ABC triblock copolymers. Three different experimental phenomena can be observed in these AB/CD mixtures by strong hydrogen bonding, as shown in Fig. 7: (a) 2 + 2 = 3 phase, (b) 2 + 1 = 3 phase, and (c) 1+1 = 2 phase [28,61–64]. For instance, Matsushita et al. blended PI-*b*-P2VP (AB) with PVPh-*b*-PS (CD), where the binary pair of P2VP/PVPh (B/C) exhibited strong hydrogen bonding; however, the PI/PS (A/D) segments

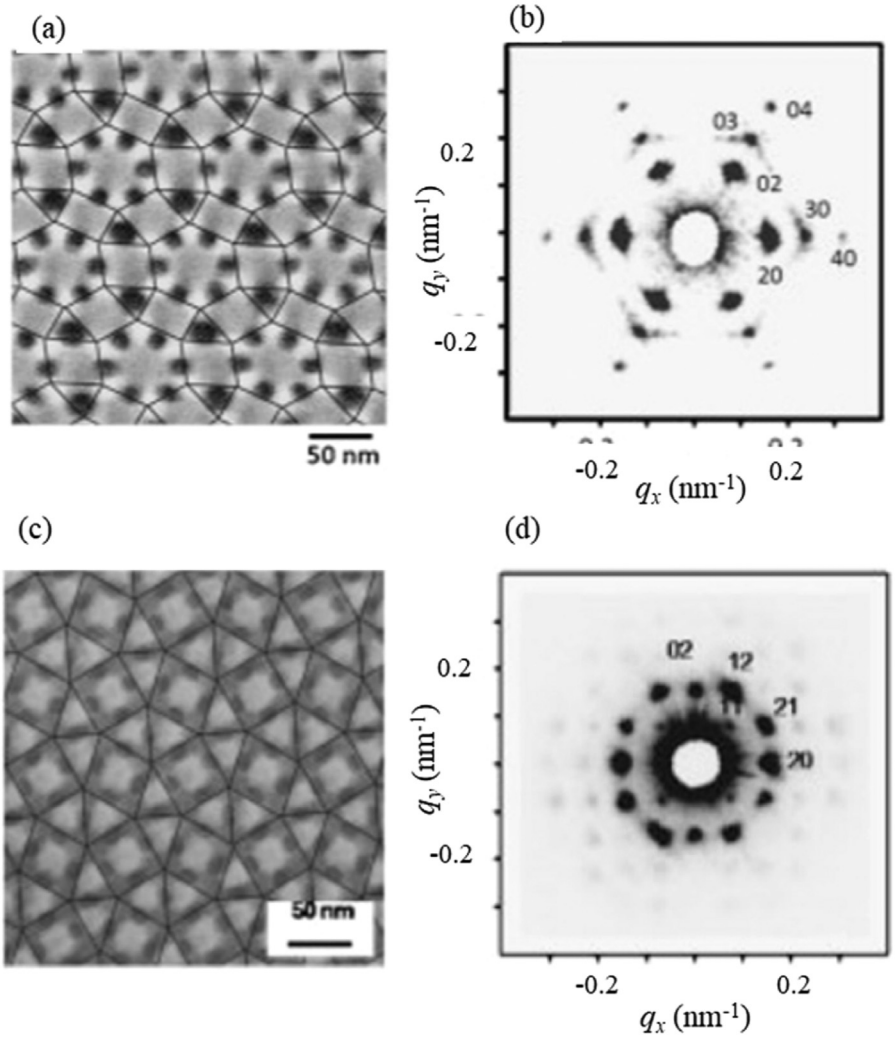

Fig. 6

(a, c) TEM images and (b,d) their corresponding micro-beam 2D SAXS pattern of (a, b) the $PI_{1.0}$-*b*-$PS_{1.8}$-*b*-$P2VP_{2.0}$ type of star triblock copolymer exhibited (3,4,6,4) and (c, d) the $PI_{1.0}$-*b*-$PS_{2.3}$-*b*-$P2VP_{2.0}$ type of star triblock copolymer exhibited (3^2,4,3,4) tiling pattern, respectively. (Adapted from Ref. [22] with permission; copyright 2007, American Chemical Society).

were immiscible. This AB/CD mixture exhibited two structures, namely, lamellae within lamellae and isolated cylinder between lamellae layers [59]. We also proposed the blending of PCL-*b*-P4VP or PMMA-*b*-P4VP (AB) with PVPh-*b*-PS (CD), and although PVPh could interact with both P4VP and PCL/PMMA segments, the competitive hydrogen bonding interaction could induce several hierarchical structures, such as core/shell cylinders, cylinders in lamellae, and core-shell double gyroid, by mediating the volume fraction and blend composition [60–64]. These systems can all be classified as 2 + 2 = 3 phase systems, as shown in Fig. 7(a) [59,60]. The second system, which is a 2 + 1 = 3 phase system as shown in Fig. 7(b), can be observed when immiscible AB is blended with miscible CD, such as PS-*b*-PVPh/P4VP-*b*-PEO or PS-*b*-P4VP/PVPh-*b*-PMMA. In these AB/CD mixtures, three-phase lamellae and core-shell cylinder structures can be observed, also mediated by competitive hydrogen bonding interactions [61,62,64]. The third system, which is a 1 + 1 = 2 phase system in Fig. 7(c), can be observed from two disordered diblock copolymers because of miscible behavior, such as PEO-*b*-P4VP/PVPh-*b*-PMMA mixtures. This system features one miscible binary pair (PVPh/P4VP) and another PEO/PMMA miscible domain, displaying lamellae and worm-like structures [63]. Based on these results, it is clear that simple blending with AB with CD diblock copolymers through hydrogen bonding cannot produce Archimedean tiling patterns.

Blending of more complex block copolymers such as diblock copolymers with triblock copolymers has also been investigated. Abetz and colleagues, for example, blended PS-*b*-PB-*b*-PtBMA (ABC) triblock copolymer featuring varying degrees of hydrolysis of the PtBMA block segment with P2VP-*b*-PCHMA or PS-*b*-P2VP (DE) diblock copolymer, resulting in the creation of various hierarchical structures, including cylinder within lamellae structures [65]. Additionally, Matsushita et al. proposed the blending of PI-*b*-P2VP-*b*-PI (ABA) triblock copolymer with PVPh-*b*-PS (CD) diblock copolymer, where the miscible binary pair of P2VP/PVPh (B/C) with strong hydrogen bonding, while PI/PS

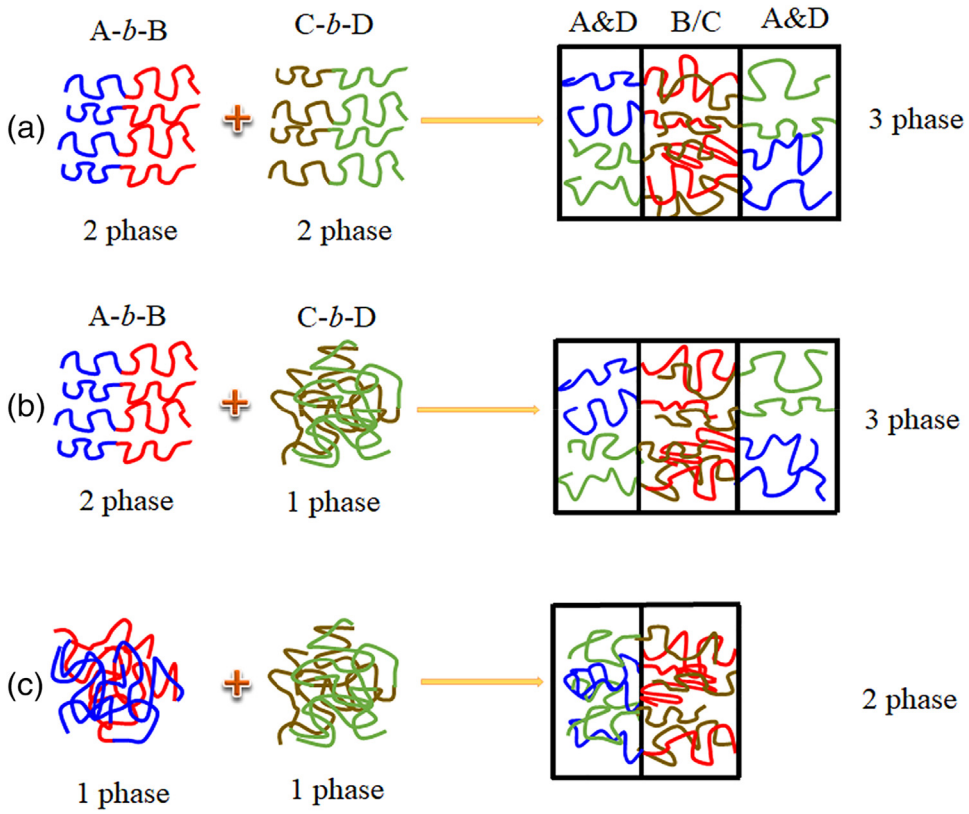

Fig. 7

Three different types of hydrogen bonding stabilized A-*b*-B/C-*b*-D mixtures of (a) 2 + 2 = 3 phase, (b) 2 + 1 = 3 phase, and (c) 1 + 1 = 2 phase [28].

(A/D) were immiscible. This blend yielded (3^3,4^2) and (3,4,6,4) Archimedean tiling patterns, as shown in Fig. 8(a)-(d) [66].

Furthermore, they also reported the combination of a PI-*b*-PS-*b*-P2VP (ABC) star triblock copolymer and a PVPh-*b*-PMMA (DE) diblock copolymer, where the miscible P2VP/PVPh (C/D) binary pair with a strong hydrogen bonding, while each PS, PI, and PMMA binary pair was immiscible. This mixture resulted in the formation of a (4,8^2) Archimedean tiling pattern, as shown in Fig. 9 [67].

3 Archimedean tiling patterns based on Frank-Kasper phases from surfactant, block copolymers and giant amphiphiles

In addition to block copolymer mixtures, Archimedean tiling patterns have also been observed in other materials, such as the Frank-Kasper (FK) phases in certain metal alloys [68]. These phases are characterized by a characteristic length scale of approximately 1 nm and highly ordered local lattices composed of topologically close-packed polyhedra. These polyhedra have coordination numbers of 12, 14, 15, and 16, and at least one polyhedron with a coordination number greater than 12. However, these polyhedra are not always perfectly regular, as regular polyhedra cannot fill space without some degree of distortion. There are currently 28 known types of FK phases, including but not limited to C14, C15, A15, σ, Z and H phases. These unique phases which have been found experimentally in a variety of soft matters, involving block copolymers, surfactants, liquid crystals, giant amphiphiles, and dendrimers [69–79]. These soft matter systems also undergo self-assembly to form spheroidal micelles that then arrange into supramolecular structures, similar to the process in metal alloys. The FK σ, A15, H, and Z phases correspond to the (3^2,4,3,4), (4^4), (3^3,4^2), and (3^6) tiling numbers, respectively, as summarized in Fig. 10 [80].

For many years, only the BCC or FCC structures were observed and predicted in asymmetric compositionally diblock copolymers, as shown in Fig. 2. However, FK σ and A15 phases have also been found in block architectures or conformations with asymmetry. Nonlinear architectures, such as ABn "miktoarm" stars or ABCA, were initially thought to be the only way to approach FK phases. But recently, simple linear diblock copolymers featured different statistical block segment lengths and architectural asymmetry have been studied to develop FK σ and A15 phases [81–84]. Bates et al. proposed a simple PDDA-*b*-PLA linear diblock copolymer with a minority volume fraction of LA segment (f_L = 0.25–0.33) that was found to create A15 phase from SCFT calculations (Fig. 11(a)) and SAXS experimental results, as shown in Fig. 11(b) [85].

The PI-*b*-PLA linear diblock copolymer with f_L = 0.15 was also found to exhibit C14 and C15 phases [69]. Ryu et al. synthesized various compositionally asymmetric PDMS-*b*-PTFEA with f_{TFEA} = 0.131-0.254 that formed FK σ and C14 phases based on SAXS analyses [86]. Chen et al. reported the simple PDMS-*b*-P2VP linear diblock copolymer with a minority P2VP volume fraction (f_{2VP} = 0.135), which displayed the FK C14 phase due to

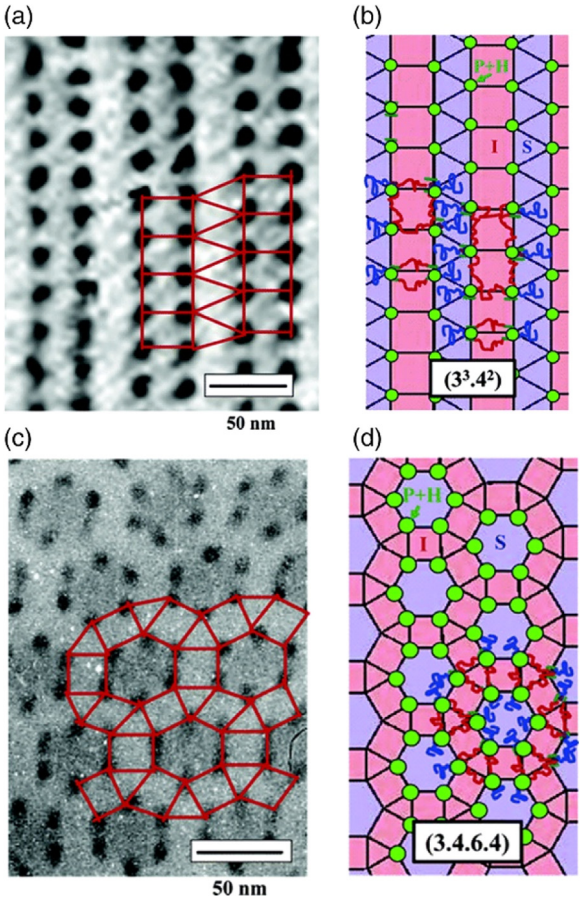

Fig. 8

Two different Archimedean tiling patterns from $PVPh_{10}$-*b*-S_{90}/PI_{90}-*b*-$P4VP_{10}$-*b*-PI_{90} blends of (a) a TEM image and (b) the schematic illustrating of the tiling (3^3,4^2) pattern of the 1/1 blend and (c) a TEM image of tiling (3,4,6,4) pattern and (d) its corresponding schematic representation of the 2/1 blend. (Adapted from Ref. [66] with permission; copyright 2018, American Chemical Society.

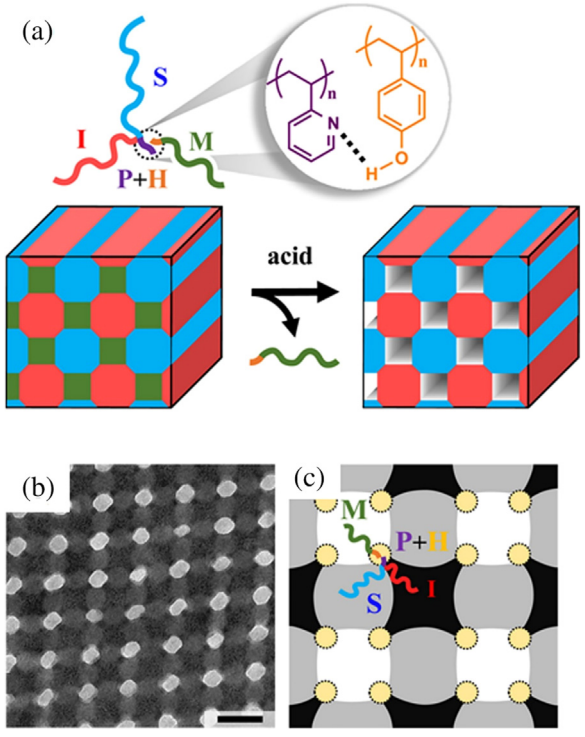

Fig. 9

(a) A scheme illustrating of star ABC triblock copolymer of PI-*b*-PS-*b*-P2VP blended with D-*b*-E diblock copolymer of PVPh-*b*-PMMA stabilized through interaction involving hydrogen bonding. (b) TEM image of ISP/HM-0.30 sample. (c) A schematic diagram based on the TEM image of the orientation of domains and chain conformation. The PVPh/P2VP domain is represented by the yellow region, while the PS, PMMA, and PI phase are represented by the gray, white, and black regions, respectively. (Adapted from Ref. [67] with permission; copyright 2018, American Chemical Society).

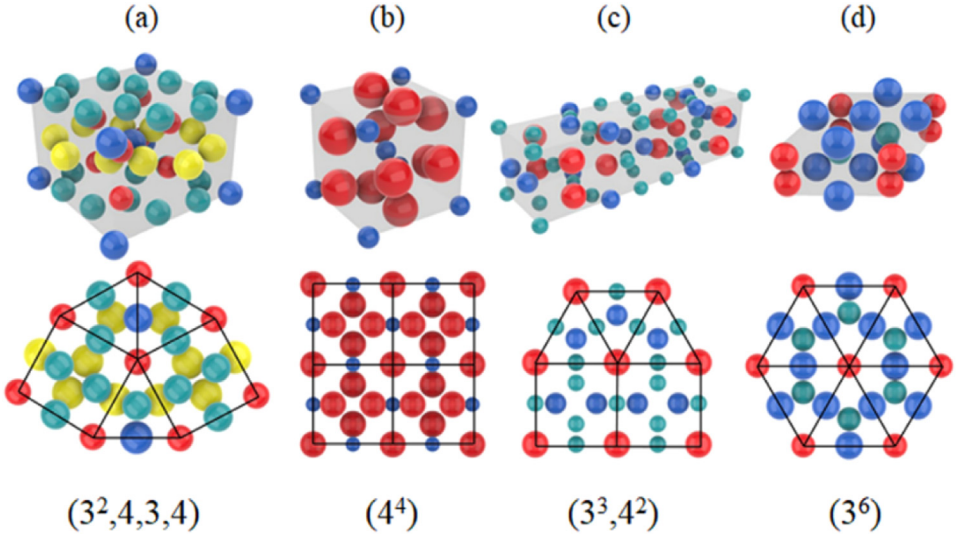

Fig. 10

The FK σ, A15, H, and Z phases correspond to the (a) (3^2,4,3,4), (b) (4^4), (c) (3^3,4^2), and (d) (3^6) tiling numbers, respectively [80].

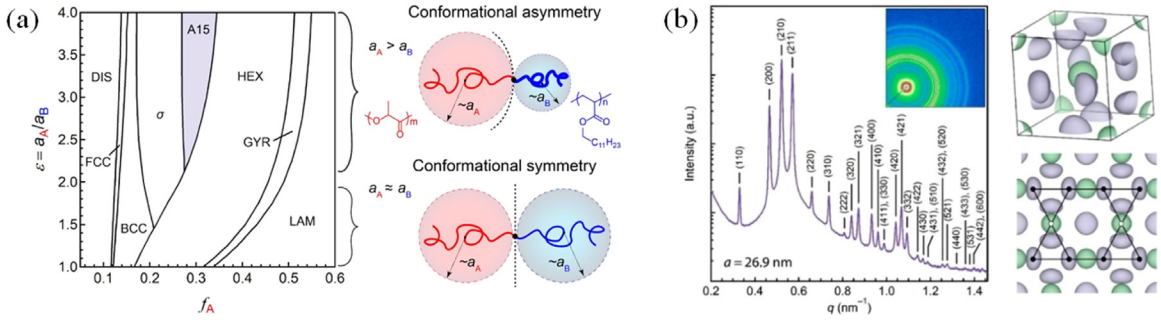

Fig. 11

(a) SCFT simulations with a χN value of 40, suggesting the A15 phase would be preferred phase in A-B diblock copolymers with a significant degree of conformational asymmetry of $\varepsilon > 2.1$ of PDDA-*b*-PLA linear diblock copolymer and (b) SAXS pattern of A15 phase obtained from PDDA-*b*-PLA linear diblock copolymer [85]. (Adapted from Ref. [85] with permission; copyright 2019, from National Academy of Sciences USA).

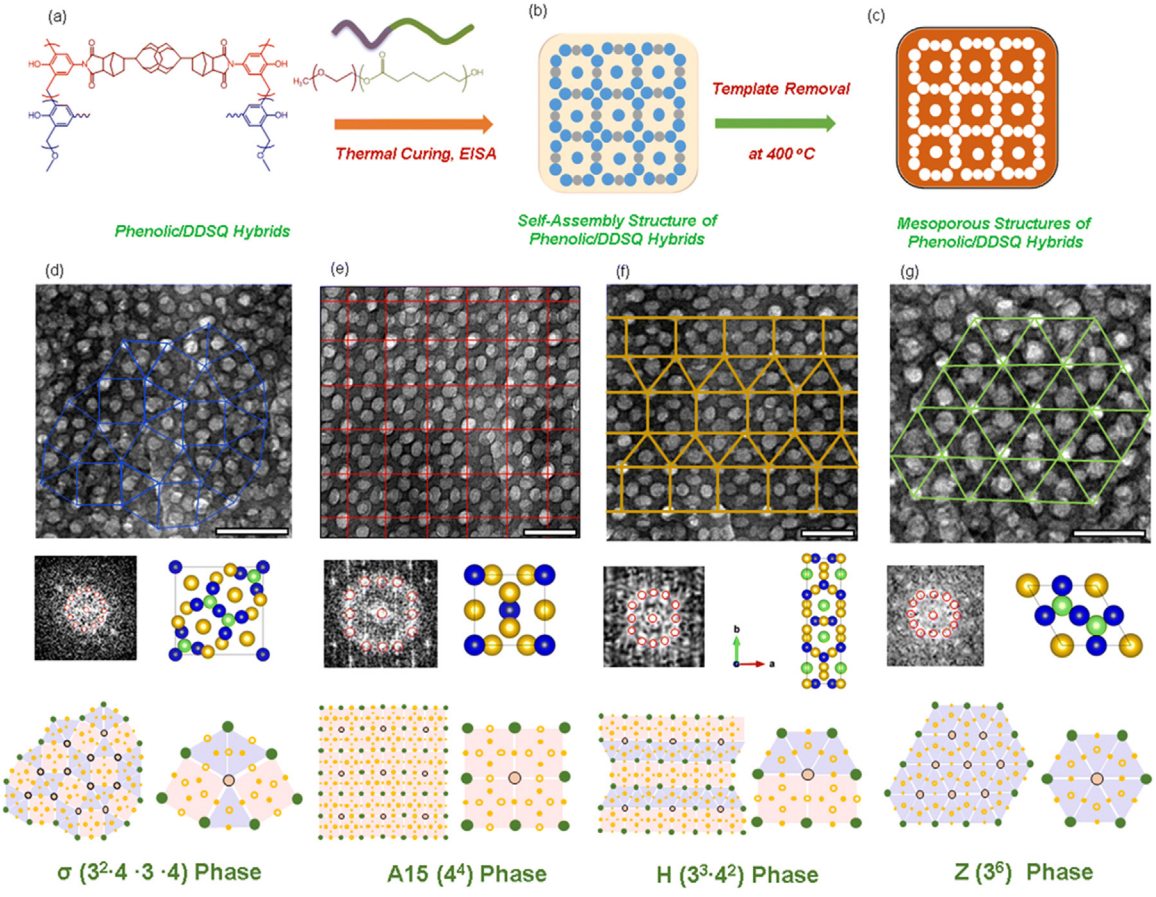

Fig. 12

(a) The chemical structure of PDDSQ hybrids, (b) a self-assembled structured formed by using PEO-*b*-PCL as a template, (c) mesoporous PDDSQ hybrids were formed after removing the PEO-*b*-PCL template, (d-g) TEM images and FFT patterns are shown for corresponding mesoporous PDDSQ hybrids exhibiting FK phases of (d) σ phase with a tiling number of (3^2,4,3,4) for PDDSQ-20, (e) A15 phase with a tiling number of (4^4) for PDDSQ-30, (f) H phase with a tiling number of (3^3,4^2) for PDDSQ-50, and (g) Z phase with a tiling number of (3^6) for PDDSQ-80 based on PDDSQ-*x*/PEO-*b*-PCL = 80/20 mixture [80].

the hard-core micelles created by the packing frustration of the coronal block segments [87].

Despite the challenges of forming unconventional FK phases with simple linear diblock copolymers, there is a proposed method to control the volume fraction of block segments using PS-*b*-PB diblock copolymer blending with PB homopolymer (A-*b*-B/B). This method allows for the creation of C14, C15, or σ phase through the "dry-brush" behavior of the blend. The addition of a PB homopolymer of similar molecular weight to the PB block ($\alpha = M_{B,homo}/M_{B,block} = 1.08$) leads to the formation of FK phases. However, blending with relatively lower molecular weight PB ($\alpha = 0.6$) results in the "wet-brush" behavior and a transition from BCC to HPC upon increasing PB content [88]. Blending diblock copolymers with homopolymers through strong

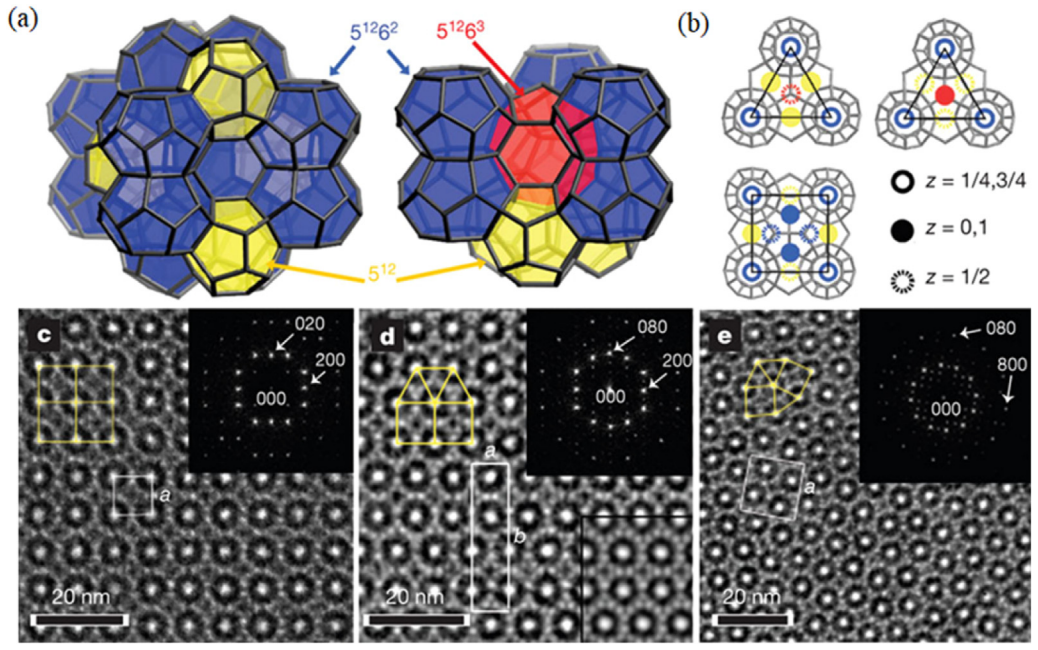

Fig. 13

(a) Three kinds of Voronoi polyhedral, (b) the projection of the polyhedral frames, indicating the 2D/3D relationship of triangles and squares, and (c-e) TEM images and their corresponding tiling numbers of (c) (4^4), (d) (3^3,4^2) and (e) (3^2,4,3,4) [94]. (Adapted from Ref. [94] with permission; copyright 2002, Nature).

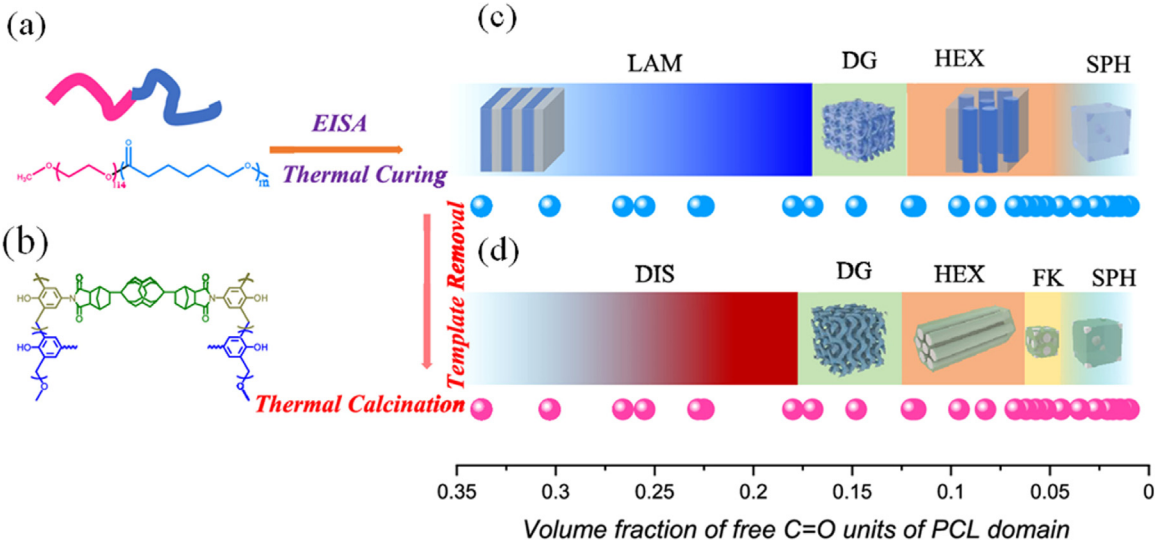

Fig. 14

(a) PEO-*b*-PCL as templates, (b) PDDSQ hybrids using EISA and thermal curing in the formation of (c) PDDSQ/PEO-b-PCL blends and (d) mesoporous PDDSQ hybrids after remove EC templates. (Adapted from Ref. [95] with permission; copyright 2022, American Chemical Society).

hydrogen bonding (A-*b*-B/C) in A/C, B/C or A/B binary pairs can also induce the wet-brush behavior, even with $\alpha > 1$. For example, PS-*b*-PVPh blending with P4VP homopolymer can transform from lamellae, double gyroid, cylinder to BCC structure upon increasing P4VP concentrations [53,54]. Thus, the simple linear symmetric diblock copolymer blending with homopolymer to provide FK phase by controlling the asymmetric volume fraction of block segment remains an interesting area of study.

The use of hydrogen bonding in diblock copolymer/homopolymer (A-*b*-B/C) mixtures to synthesize mesoporous phenolic resin or silica materials (with pore sizes ranging from 2–50 nm) using diblock copolymers as templates has been extensively studied for the past twenty years, resulting in structures such as double gyroid, cylinder and BCC phases [28,89–91]. However, we have recently reported the synthesis of mesoporous FK phases (such as σ, A15, H, and Z phases) using PDDSQ (phenolic/double-decker silsesquioxane hybrids) hybrids and linear diblock copolymers of PEO-*b*-PCL as templates mediated by competitive hydrogen bonding [80]. We used PDDSQ hybrids with varying amounts of DDSQ (Fig. 12(a)) as the

matrix and PEO_{114}-*b*-PCL_{87} diblock copolymers as the template to investigate the formation of complex mesoporous FK phases as shown in Fig.s 12(b)-(c) [80,92,93].

We used PDDSQ-*x*/PEO_{114}-*b*-PCL_{87} = 80/20 blends to investigate the complex mesoporous FK phases. TEM images and FFT diffraction patterns along the [001] direction revealed the formation of the tetragonal lattice FK σ phase with a (3^2,4,3,4) tiling number using PDDSQ-20 with the lowest DDSQ composition (Fig. 12(d)). Increasing the DDSQ composition to PDDSQ-30 resulted in the formation of FK A15 phase with a typical (4^4) tiling number (Fig. 12(e)). Fig. 12(f) shows the TEM image and FFT pattern of PDDSQ-50/PEO-*b*-PCL = 80/20 mixture, which exhibited the (3^3,4^2) tiling number of the mesoporous FK H phase. Increasing the DDSQ concentration to PDDSQ-80, a mesoporous FK Z phase with the typical (3^6) tiling number was formed as shown in Fig. 12(g). By using PEO_{114}-*b*-PCL_{87} as the template and adding DDSQ concentration in PDDSQ hybrids, it was able to induce the different formation of FK σ, A15, H, and Z phases [80]. The presence of inorganic DDSQ nanoparticles enhanced the interaction parameter (χ) value in PDDSQ-*x*/PEO_{114}-*b*-PCL_{87} blends due to the intrinsic immiscibility between the organic diblock copolymer and inorganic DDSQ cage structure.

Furthermore, the use of low molecular weight surfactant, such as N-myristoyl-L-glutamic acid or CTAB, as template has also been observed to form mesoporous silica FK σ, A15, and H phases with dodecagonal tiling patterns, as shown in Fig. 13 [94].

However, the pore size obtained using these surfactants was relatively small (< 4 nm) compared to PEO-based diblock copolymers. To enhance both the pore size and the segregation strength of the χN value in PDDSQ/PEO-*b*-PCL blends, we prepared various PEO-*b*-PCL with different PCL lengths as templates and then blended with PDDSQ-25 hybrids to form mesoporous materials, as shown in Fig. 14 [95].

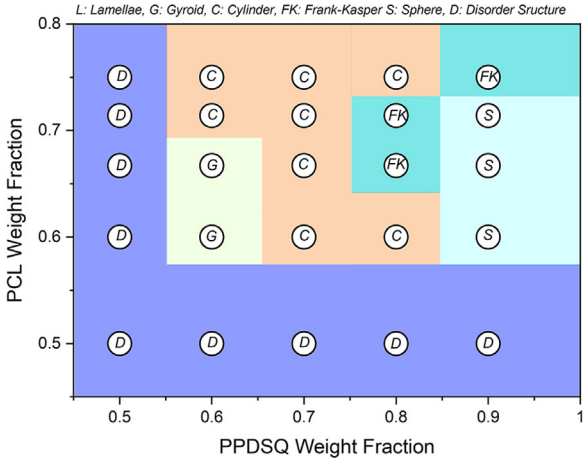

Fig. 15

Phase diagram of the different phase observed in mesoporous PDDSQ hybrids from PDDSQ/EC blends based on data obtained from TEM images and SAXS patterns. (Adapted from Ref. [95] with permission; copyright 2022, American Chemical Society).

The resulting phase diagram of those mesoporous PDDSQ hybrids exhibited high surface area and pore volume with double gyroid, cylinder, and even FK structures, which was mediated through the molecular weights of the PCL segment, as shown in Fig. 15. Notably, the mesoporous FK phase was only observed in the high molecular weight PCL blocks of PEO-*b*-PCL, due to the high χN value, which is consistent with SCFT results [85].

Recently, there has been much interest in using mono-functionalized POSS nanoparticles connected to polymer chains or various organic functional units to form giant amphiphiles or giant block copolymers and resulting in FK σ, A15, and Z

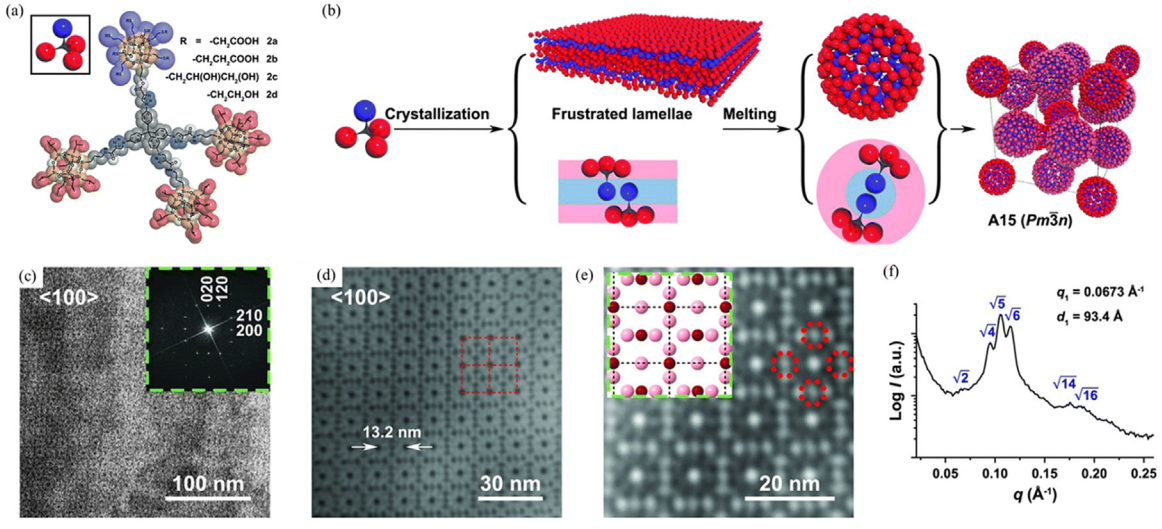

Fig. 16

(a) The giant tetrahedron composed of POSS cage featuring a chemical structure of hydrophilic blue sphere and hydrophobic red spheres, (b) the self-assembled structure to form A15 phase with a unique molecular packing arrangement, (c) a TEM image of the A15 phase, (d) Fourier filtering of TEM image has revealed the presence of a tiling number of (4^4) along the [100] direction, (e) The resulting inverse coloring of the filtered image highlights in (d), which come in different sizes, and (f) SAXS profile of this giant tetrahedron. (Adapted from Ref. [96] with permission; copyright 2015, Science).

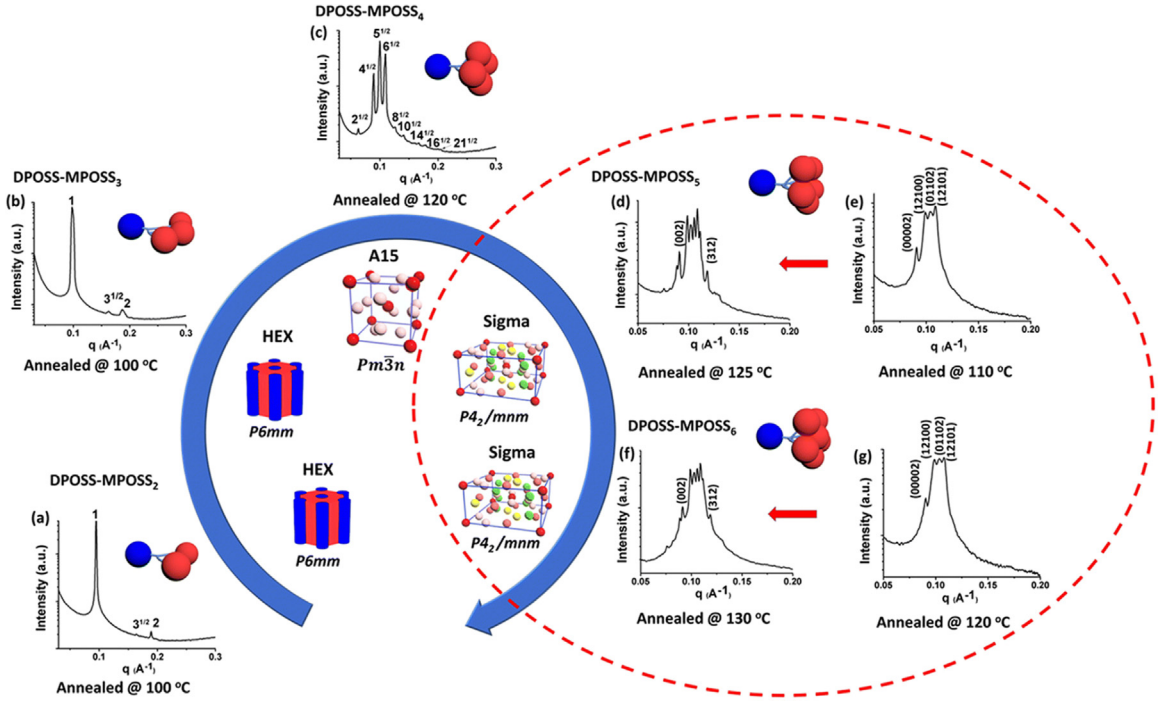

Fig. 17

The phase behavior of various dendron-like AB_n giant surfactants, including (a) DPOSS-MPOSS$_2$ and (b) DPOSS-MPOSS$_3$ with HPC structure, (c) DPOSS-MPOSS$_4$ with A15 phase, (d-e) DPOSS-MPOSS$_5$ with DQC phase after annealing at 110°C (d) and σ phase after annealing at 125°C (e), (f-g) DPOSS-MPOSS$_6$ with DQC phase after annealing at 120°C (f) and σ phase after annealing at 130°C (g). (Adapted from Ref. [98] with permission; copyright 2019, American Chemical Society).

phases. For instance, Cheng et al. developed a giant amphiphilic tetrahedron using one hydrophilic and three hydrophobic POSS nanoparticles (Fig. 16(a)), which could self-assemble into the FK A15 phase as shown in Fig. 16(b)-(e). The analysis of TEM showed a typical (4^4) tiling number along the [001] zone. The SAXS analysis also confirmed the A15 phase with the peak ratio of $\sqrt{2}$: $\sqrt{4}$: $\sqrt{5}$: $\sqrt{6}$, as shown in Fig. 16(f) [96].

They also reported the formation of giant molecules consisting of six POSS nanoparticles on a triphenylene core that exhibited a typical (3^6) tiling number and could self-assemble into FK Z phase [97]. Moreover, the DPOSS-MPOSSn dendron giant amphiphilic surfactant with hydrophilic MPOSSn (n is the number of MPOSS) and hydrophobic DPOSS nanoparticles could self-assemble into cylinder, A15, and σ phase upon increasing the n value, as shown in Fig. 17 [98].

A multi-branched OP8 and OP14 with eight and fourteen isooctyl POSS nanoparticles connected by click reaction also exhibited self-assembled structures from DQC, DDQC, and σ phases in these giant surfactant mixtures [99]. Additionally, long chain PS with different topologies as hydrophobic tails with POSS nanoparticle as hydrophilic head were synthesized as the DPOSS-NPS$_m$ giant surfactants. The FK and quasicrystal structures were observed in various regions with typical BCC, DDQC, σ, and A15 phases, which are highly dependent on their molecular geometry (Fig. 18(A)-18(M)). The phase diagram of these DPOSS-NPS$_m$ giant surfactants was summarized in Fig. 18(N). Other POSS-based giant surfactants were also prepared, and FK and quasicrystal structures were observed under different conditions [100].

4 Archimedean tiling patterns based on covalent organic frameworks (COFs)

Yaghi et al. proposed the discovery of COFs, which are porous organic polymers with 2D or 3D crystalline structures [6,101,102]. These materials are synthesized using reversible reactions between building monomers that are connected by robust covalent bonds with light elements. The covalent bonds in COFs provide self-healing ability and thermodynamic control, which results in long-range ordered crystalline properties and outstanding chemical stability under basic and acidic conditions, as well as in organic solvents. These unique properties make COFs promising materials for various applications including energy storage, optoelectronic devices, catalysis, drug delivery, and gas capture [103–109].

Fig. 19 illustrates various topologies of 2D COF materials that have been synthesized using different building units and approaches [110]. The design of COFs is based on the principles of geometry and dimension of the building blocks, which allows for the prediction of their topologies. COFs are distinct from other organic porous materials [111–113] like conjugated microporous polymers (CMP) [114–116], hyper-crosslinking polymers (HCP) [117–120], and covalent triazine frameworks (CTFs) [121–123] due to their ability to form crystalline structures that can be corrected and rearranged through reversible covalent bonds.

Initially, Yaghi et al. used boronic acids and catechols to connect building units in COFs, but these structures were prone to hydrolysis [6,101,102]. To overcome this issue, alternative synthetic routes were developed that introduced stable imino bonds through the condensation of amine and aldehydes, as well as azine, hydrazones, and imides. Fig. 20 summarizes the

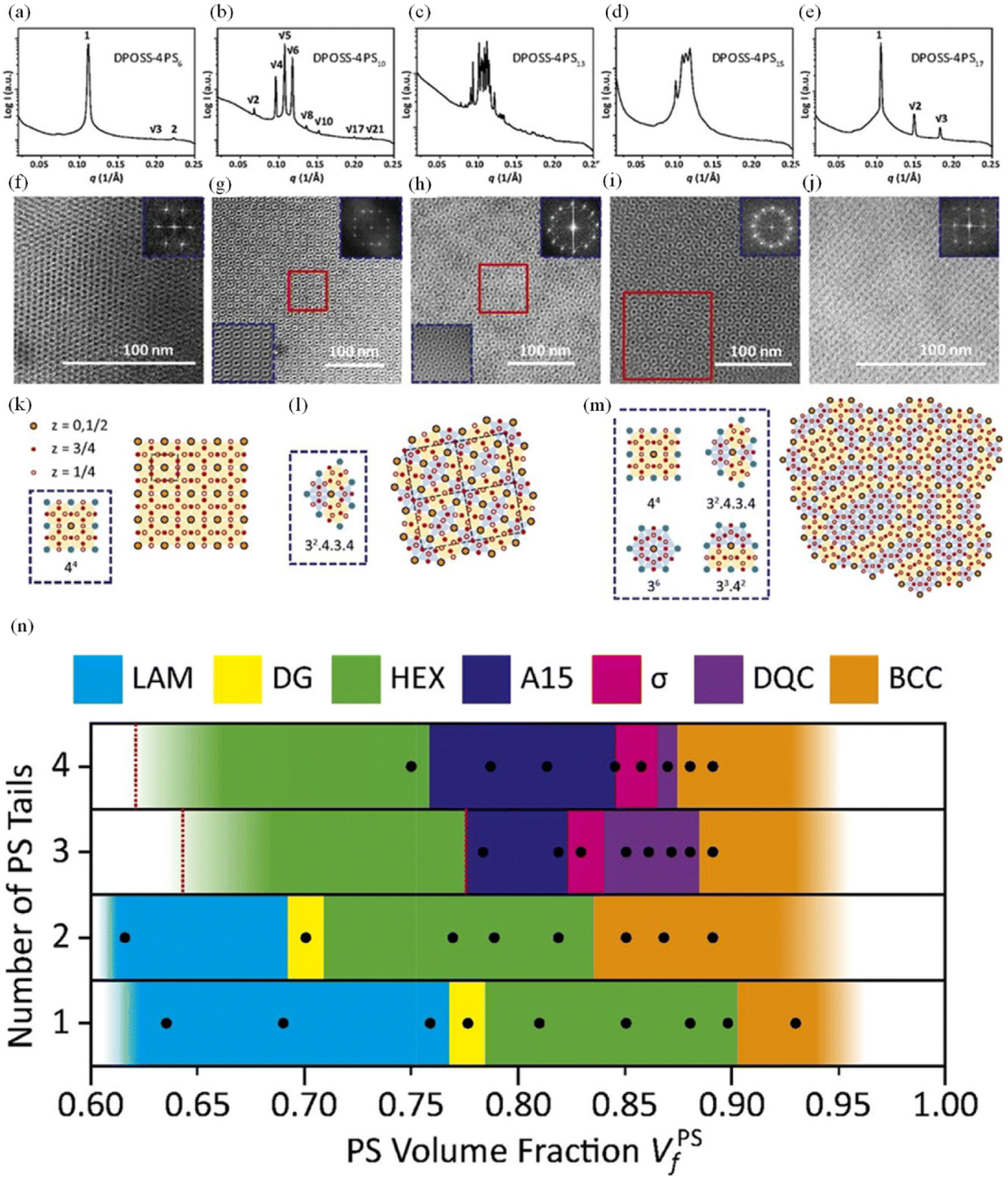

Fig. 18

Various DPOSS-4PS$_m$ species analyzed by SAXS, TEM, FFT, and Fourier filtering techniques and exhibited different phases: (a, f) HPC phase observed in DPOSS-4PS$_6$, (b, g) A15 phase presented in DPOSS-PS$_{10}$, (c, h) σ phase found in DPOSS-4PS$_{13}$, (d, i) DQC phase identified in DPOSS-4PS$_{15}$, and (e,j) BCC phase seen in DPOSS-4PS$_{17}$.,(g-i) 2D tilting patterns indicated by the red-line box include: (k) A15, (l) σ, and (m) DQC phase, and (n) the experimental phase diagram for the DPOSS-nPS$_m$ giant surfactant. (Adapted from Ref. [100] with permission; copyright 2016, from National Academy of Sciences USA).

commonly used organic reactions in COF synthesis, including boroxine, boronic ester, imine, hydrazine, azine, β-ketoenamines, imide, triazine, urea, and squaraine bonds [110]. To enhance the chemical stability of COFs, robust networks have been created that can avoid strong acids and bases, such as the synthesis of β-ketoenamines using primary amines and TFP-3OHCHO through an irreversible enol-keto tautomerization process [124–126].

The architecture and size of the pores in COFs are determined by matching the geometry of building blocks to create polygonal frameworks. The dimensions and geometry of the linkers used influence the shape of the polygons and the pore size. For instance, a hexagonal COF can be produced by combining the building block with C_3-symmetry and the linear linker with C_2-symmetry ($C_3 + C_2$) (Fig. 19(c)). Additionally, hexagonal COFs can

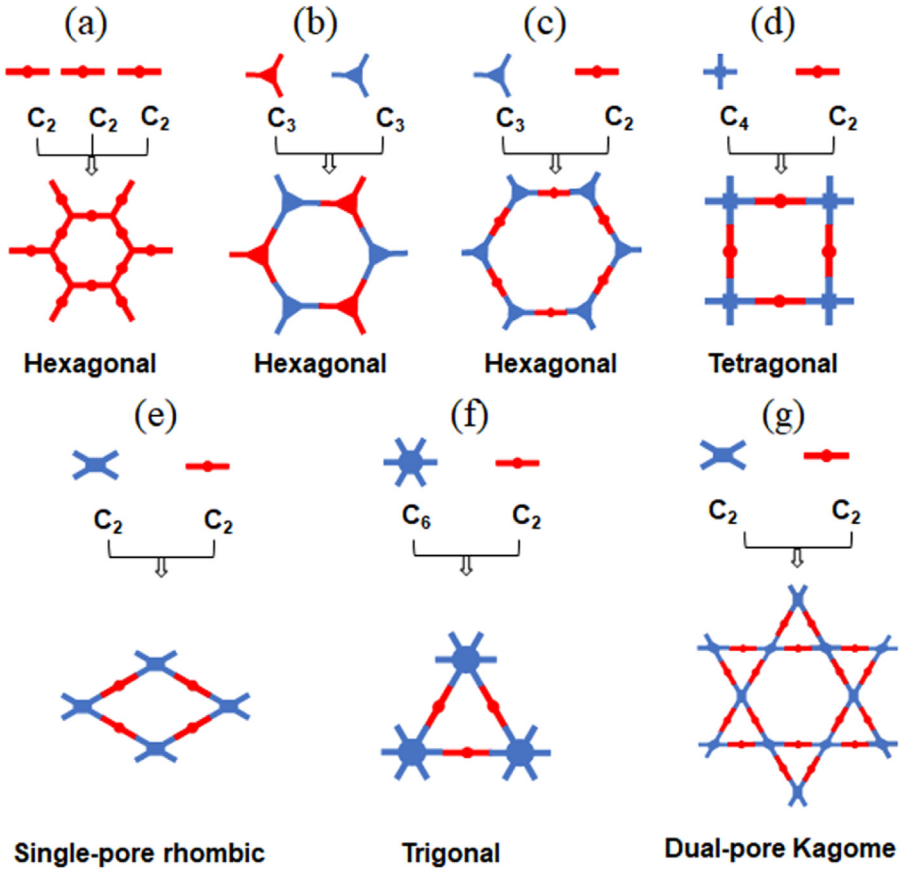

Fig. 19

Topology diagrams that serve as a foundational framework for COF design and the assembly of 2D COFs [110].

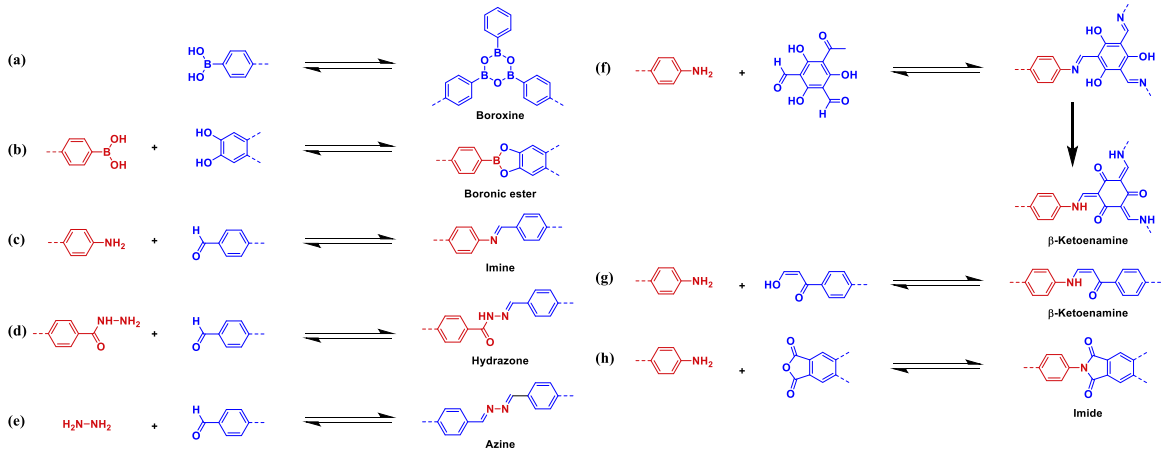

Fig. 20

Condensation reactions involving commonly utilized linkages in COFs include: (a) boroxine, (b) boronic ester, (c) imine, (d) hydrazone, (e) azine, (f,g) β-ketoenamine, (h) imide [110].

be formed by using the self-condensation of a C_2-symmetric unit (Fig. 19(a)) or by utilizing two building blocks with the trigonal planar C_3 + C_3 geometry (Fig. 19(b)). This topology of COFs corresponds to the Archimedean hexagonal tiling (6^3) pattern, which is the most common structure observed in COF materials [127–130]. For example, we synthesized two types of 2D TPA-COFs and TPT-COFs using one-pot polycondensation methods. We used TPA-3NH_2 and TPT-3NH_2 as starting materials, along with various triarylaldehydes that differed in nitrogen content, symmetry, and planarity (Fig. 21) [130]. The resulting COFs displayed excellent properties, such as large surface areas (>1700 m^2 g^{-1}) and high crystallinity with outstanding thermal stability. The degree of

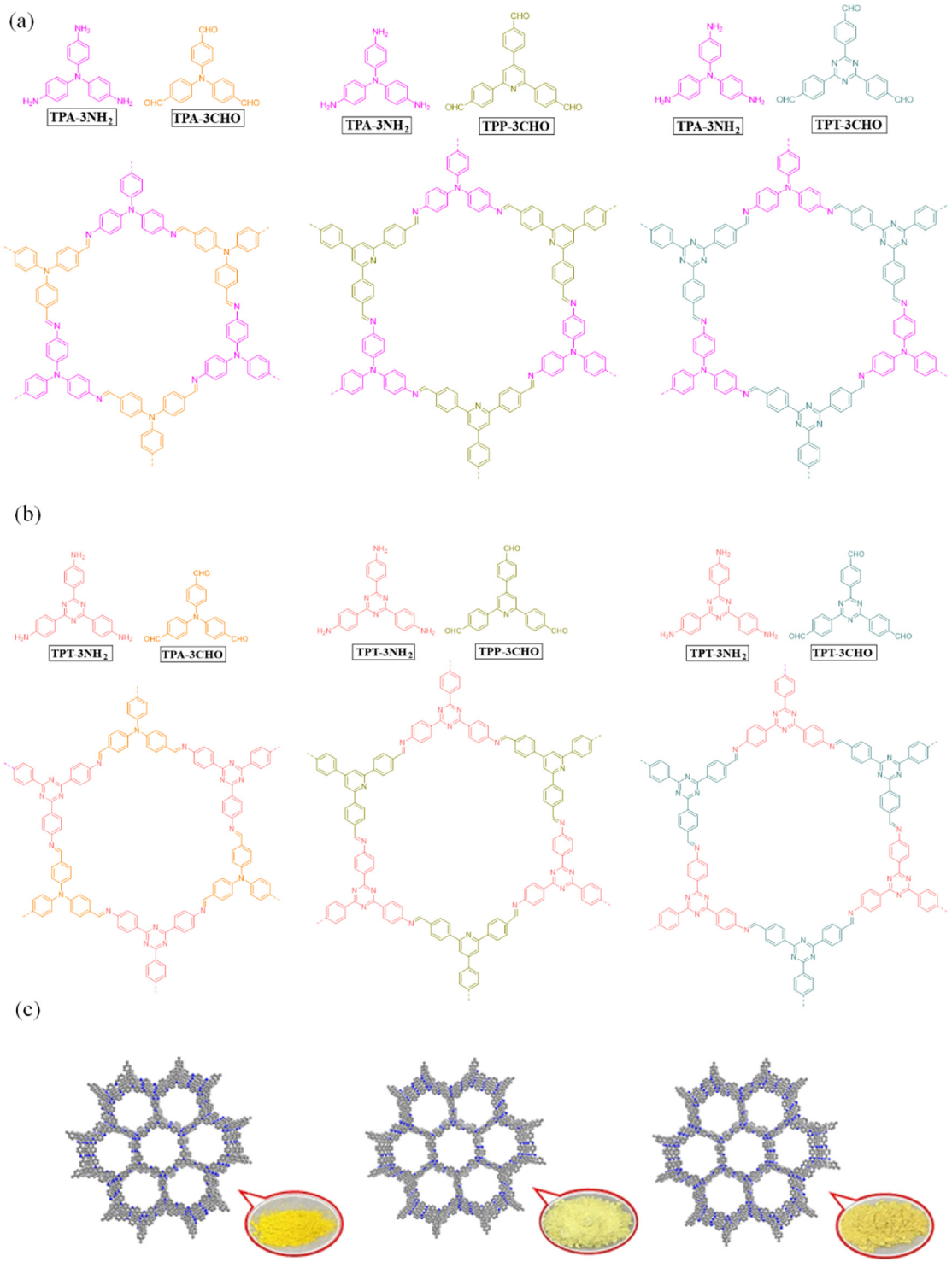

Fig. 21

Synthesis strategies for three isoreticular 2D COFs: (a) TPA-COFs derived from tiphenylamine and (b) TPT-COFs obtained from triphenyl triazine, both using three aldehyde units with varying planarities, and (c) a 2D simulation structure of TPT-COFs. The color code represents carbon in gray and nitrogen in blue with tiling number of (6^3) [130].

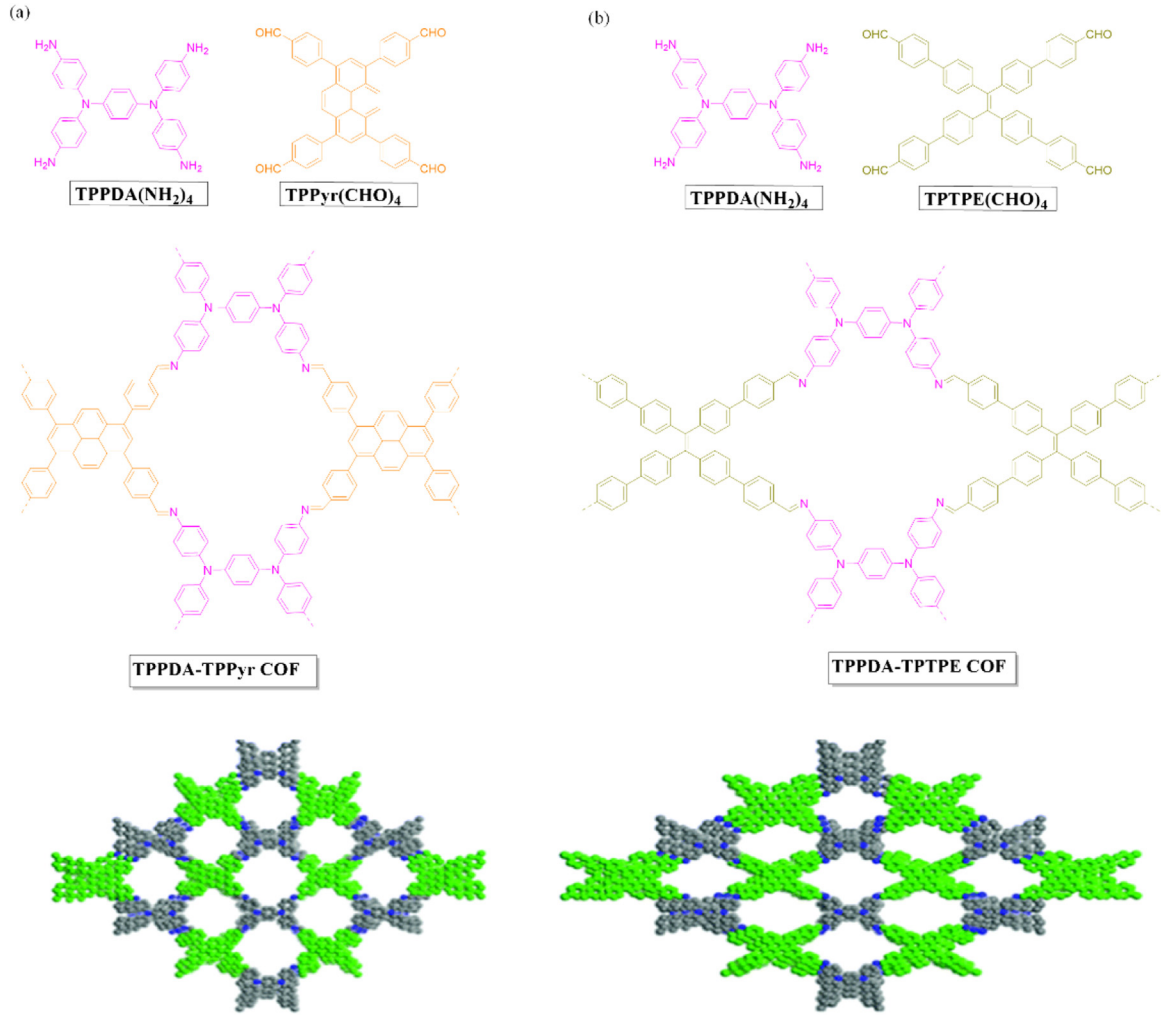

Fig. 22

Syntheses and chemical structure of (a) TPPDA-TPPyr COF and (b) TPPDA-TPTPE COF with tiling number of (4^4) [134].

crystallinity and surface area of these COFs featuring hexagonal tiling (6^3) pattern were significantly impacted by the symmetry and planarity of the triarylaldehydes used in the synthesis [130].

The creation of tetragonal pores with an Archimedean square tiling (4^4) pattern in COFs is achieved by combining tetragonal building blocks with linear linkers ($C_4 + C_2$) (Fig. 19(d)) [110] or other tetragonal building units ($C_4 + C_4$) [131–133]. These pores form elongated 1D channels within stacked layers that extend in two directions, which allows for the creation of various π-conjugated frameworks. For instance, we synthesized a redox-active triphenyl-amine derivative TPPDA(NH_2)$_4$ featuring tetraformyl linker and utilized it to produce TPPDA-TPPyr or TPPDA-TPTPE COF, through [C_2+C_2] condensation (Fig. 19(e)) [134]. These TPPDA-COFs showed excellent crystallinity, thermal stability, and high surface areas. Moreover, due to the presence of redox-active triphenylamine units in their chemical structures, the TPPDA-COFs with a square tiling pattern (4^4) exhibited excellent electrochemical capacitances (Fig. 22).

To produce 2D COFs with high-density π-units and micropores, a $C_6 + C_2$ topology scheme was utilized. This approach allowed for the creation of triangular lattices, which can be assigned the Archimedean triangular tiling (3^6) pattern (Fig. 19(f)). This method results in COFs with highly dense π-units and smaller pores than those produced by other topology diagrams. For example, Jiang et al. successfully synthesized two triangular COFs, HPB-COF and HBC-COF, through various C_6-symmetric vertices with the Archimedean triangular tiling (3^6) pattern (Fig. 23) [135]. The resulting COFs exhibited excellent thermal and solvent stabilities, as well as supermicropores with pore sizes < 1.2 nm. This enabled both inter- and intar-layer π-cloud delocalization. Furthermore, the researchers observed significant photoconductivity in these COFs, demonstrating their potential use in optoelectronic applications. Typically, microporous COFs are produced using a trigonal structure, while tetragonal and hexagonal topologies are useful for suggesting mesopores [136].

The majority of COFs reported in the literature have a 2D layered structure that can be synthesized using various modular-pattern polymerization approaches, such as [$C_3 + C_2$], [$C_3 + C_3$], [$C_4 + C_2$], [$C_4 + C_4$], and [$C_6 + C_2$], as mentioned previously.

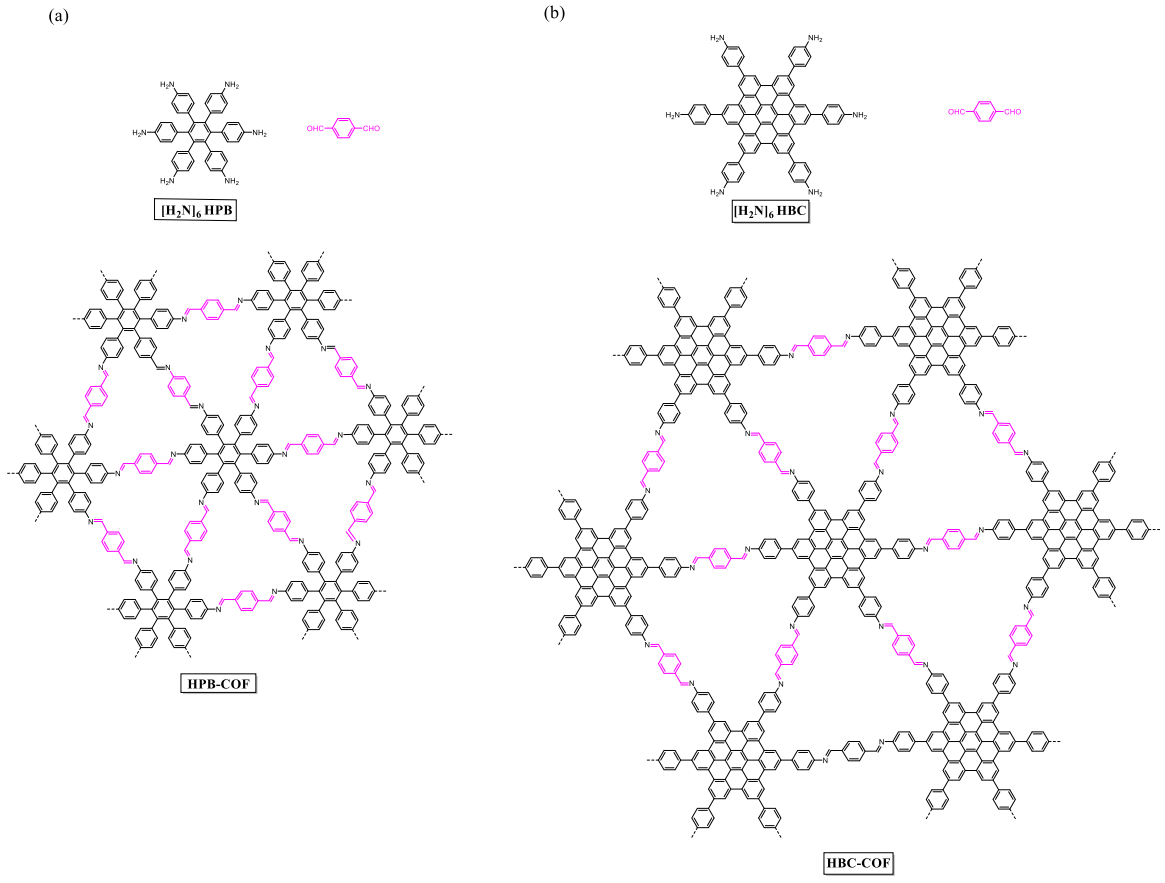

Fig. 23

(a) the synthesis of imine-linked triangular HPB-COF and (b) and HBC-COF with tiling (3^6) pattern and accompanied by its model reaction [135].

These strategies have resulted in a variety of topologies, most commonly featuring hexagonal (6^3), square (4^4), and triangle (3^6) with regular Archimedean tiling for 2D COFs. Despite efforts to reticulate more than two types of organic linkers or vary edge lengths and vertex angles to desymmetrize pore structures, creating 2D COFs with new topologies featuring semiregular Archimedean tiling remains a significant challenge. Zhao et al. addressed this challenge by creating the first heteropores of SIOC-COF, with two different pore sizes including trigonal micropore and hexagonal mesopore by combining ETTA (the D_{2h}-symmetric unit) with *p*-phthalaldehyde as the C_2-symmetric unit (Fig. 19(g)) to form a Kagome structure with a trihexagonal tiling (3,6,3,6) pattern, as shown in Fig. 24(a). This dual pore size of SIOC-COF was confirmed by using the comparison of experimental and simulated X-ray diffraction patterns for this SIOC-COF with eclipsed stacking (AA) and a N_2 adsorption/desorption isotherm also exhibited two modes of I and IV types [Fig. 24(b)], which are due to microporous and mesoporous behaviors with two narrow pore size distributions centered at 0.73 and 2.52 nm, respectively [Fig. 25(c)] [137]. This achievement demonstrates the potential for creating 2D COFs with new topologies and unique pore structures, which could have important implications for various applications [138,139].

To understand the structural diversity of 2D COFs, researchers have also made significant efforts to reticulate more than two types of organic linkers or vary the edge lengths and vertex angles to desymmetrize the pore structures. For example, Bein and co-workers used ETTA with BDT to create BDT-ETTA COF featured Kagome-type structure that worked well as the photocathode for water-splitting [140]. Zhao et al. also created heteroporous COFs by combining BABD (a C_{2v}-symmetric unit) with 1,4-diaminobenzene (DB) or benzidine (BZ) to make BABD-DB or BABD-BZ COFs with two various types of pores and shapes with trihexagonal tiling (3,6,3,6) pattern, which were used as chemosensors for nitroaromatics [141]. In addition, we proposed new Cz-BD or Cz-DHBD COFs through the condensation reaction of Cz-4CHO as a C_2-symmetric unit with BD or DHBD as a C_2-symmetric linker. It was observed that the Cz-BD COF had only single pore size with the tetragonal structure; however, Cz-DHBD COF had the Kagome structure with trihexagonal tiling (3,6,3,6) pattern featuring two types of pores as shown in Fig. 25 [142].

A novel approach to creating semiregular Archimedean tilings for 2D covalent organic frameworks (COFs) has been proposed by Cui et al. In their work, they used a pseudo five-fold symmetric building block called 1,2,3,4,5-penta(4-formylphenyl)pyrrole (PFPP), which was reacted with two linear

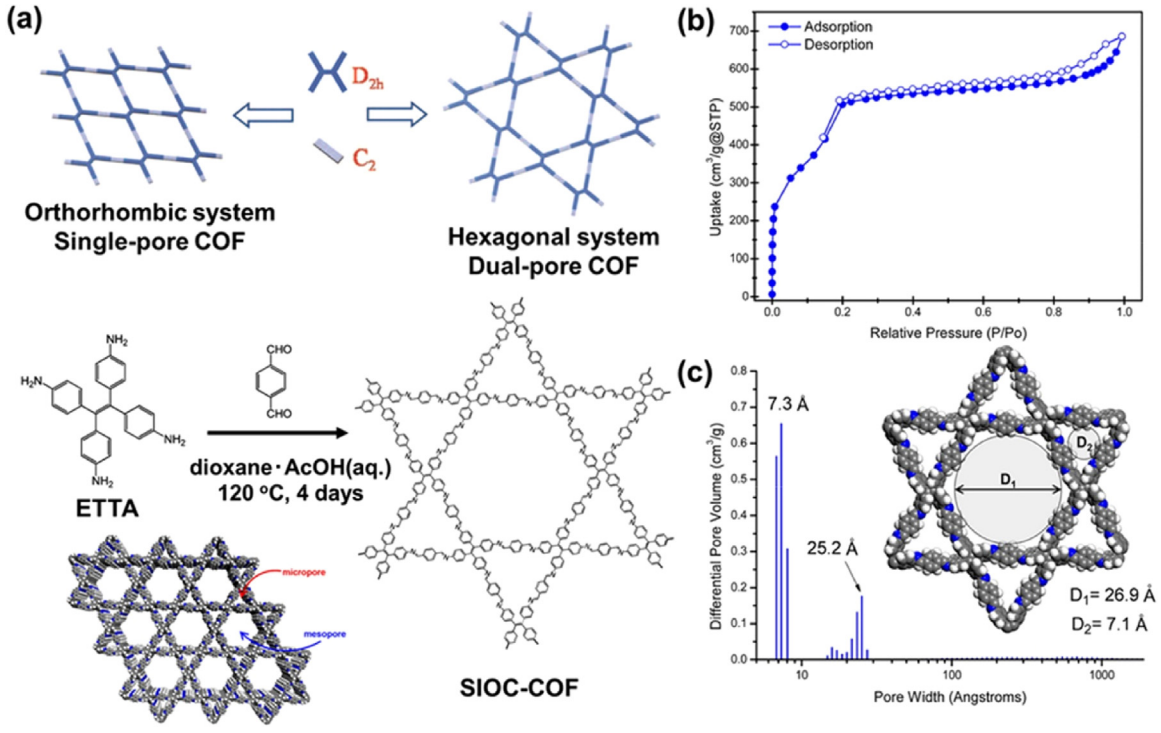

Fig. 24

(a) Synthesis process, (b) a N_2 adsorption/desorption isotherm, and (c) pore size distribution analysis for the Kagome structure with tiling (3,6,3,6) pattern of SIOC-COF [137]. (Adapted from Ref. [137] with permission; copyright 2017, Royal Society of Chemistry).

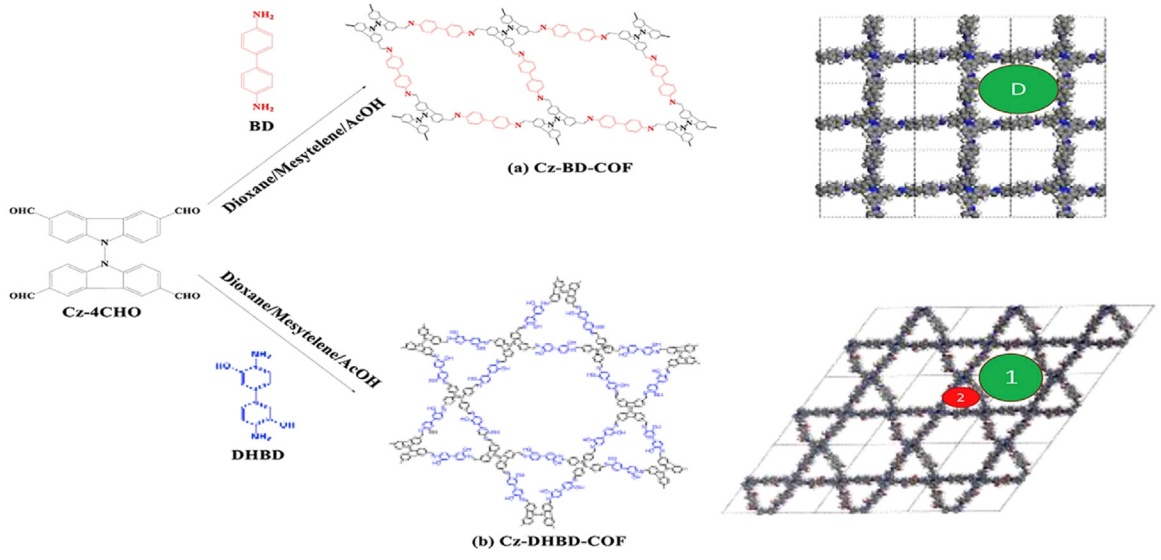

Fig. 25

Syntheses of (a) Cz-BD and (b) Cz-DHBD COFs from Cz-4CHO monomer with two different diamine monomers [142].

aromatic diamines, p-phenylenediamine and 2,5-dimethyl-1,4-benzenediamine, via a Schiff base reaction as shown in Fig. 26 [143].

This resulted in the formation of ten different tessellations with various topologies, which were compared to the Reticular Chemistry Structure Resource (RCSR) database as shown in Fig. 27. Among them, three semiregular Archimedean tilings were identified, including the truncated triangular tiling (**tts**), the snub hexagonal tiling (**fsz**), and the elongated triangular tiling (**cem**) [144].

These types of semiregular Archimedean tilings have been observed in various materials, such as alloys, nanoparticle superlattices, metal-organic frameworks (MOFs) [145], liquid crystalline networks [146], and COFs. X-ray diffraction patterns of the PFPP COF were found to match well with the simulated profile of the **cem** topology featuring an elongated triangular

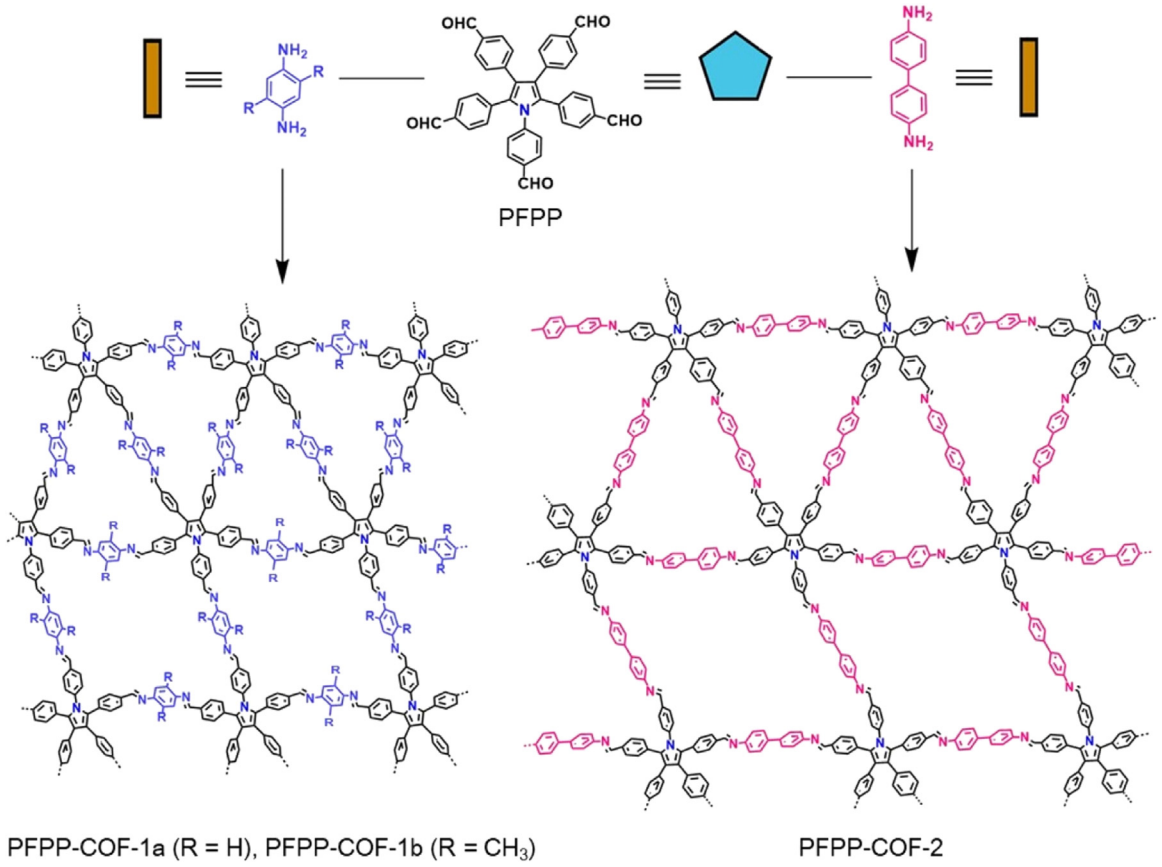

Fig. 26

Synthesis of three different 2D PFPP-COF with elongated triangular tiling ($3^3,4^2$) pattern. (Adapted from Ref. [143] with permission; copyright 2022, American Chemical Society).

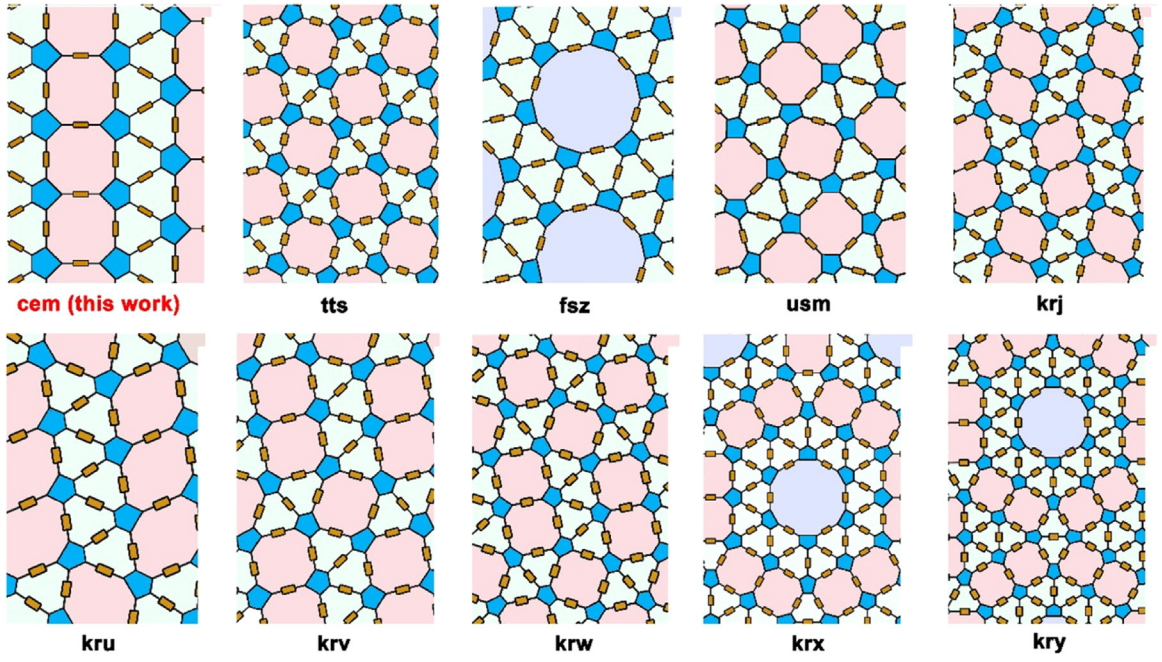

Fig. 27

Schematic representation of the (2,5)-connected 2D network featuring 10 different potential topologies. (Adapted from Ref. [143] with permission; copyright 2022, American Chemical Society).

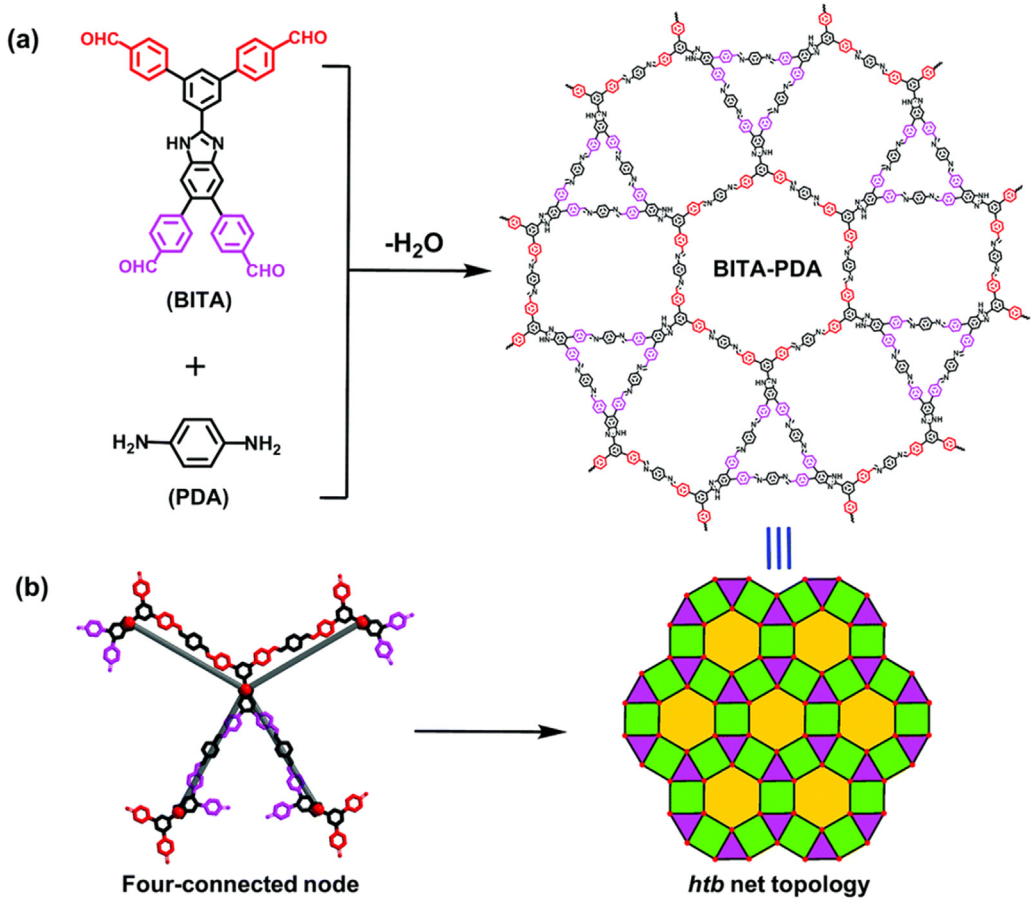

Fig. 28

(a) Chemical structures of BITA (tetra-aldehyde monomer), PDA (diamine linker) and the resulting 2D BITA-PDA COF with (3,4,6,4) Archimedean tiling, (b) a subunit of the COF emphasizing the four-connected node, which has predefined vertex angles that allow for the formation of Archimedean tiling pattern of (3,4,6,4), which is equivalent to the **htb** net topology. (Adapted from Ref. [147] with permission; copyright 2017, Royal Society of Chemistry).

tiling (3^3,4^2) with the AA stacking mode in the P-1 space group [143].

Zhang et al. have introduced a new 2D covalent organic framework (COF) material known as BITA-PDA COF, which is composed of benzimidazole-based tetra-aldehyde (BITA) with phenylenediamine (PDA) building blocks. This BITA monomer features four connected nodes with specific angles of 60, 90, 90, and 120 degrees with the neighboring linkages of its aldehyde units. This configuration is consistent with the Archimedean rhombitrihexagonal tiling (3,4,6,4) pattern, as shown in Fig. 28 [147].

BET analyses indicated the presence of three distinct pore types: trigonal (1.0 nm), rectangular (1.8 nm), and hexagonal (3.2 nm) in a diameter, which were consistent with the theoretically predicted sizes (Fig. 29) [147]. Other heteropore COFs were also observed using pore design principles with complex structures and hierarchical porosity [148,149].

5 Conclusions

This review article highlights recent advancements in the synthesis and preparation of soft materials, namely block copolymers or covalent organic frameworks, featuring Archimedean tiling patterns. These materials have garnered significant attention from academia and industry due to their meso and microporous properties that enable their use in energy and gas storage, photo-catalysis, and separation applications. The high surface area and pore volume of these materials provide them with an advantage over purely micro or mesoporous materials. While various Archimedean tiling patterns have been observed in COFs and block copolymers, there are still untapped patterns such as (3^4, 6), (3, 12^2), and (4, 6, 12) that have yet to be discovered. In addition, the direct TEM image of Archimedean tiling patterns based on COF materials is still a challenge and this field is still a hot topic with new Archimedean tilting patterns based on block copolymers and COFs because of various new possible applications in my opinion.

Declaration of Competing Interest

The authors declare that they have no known competing financial interests or personal relationships that could have appeared to influence the work reported in this paper.

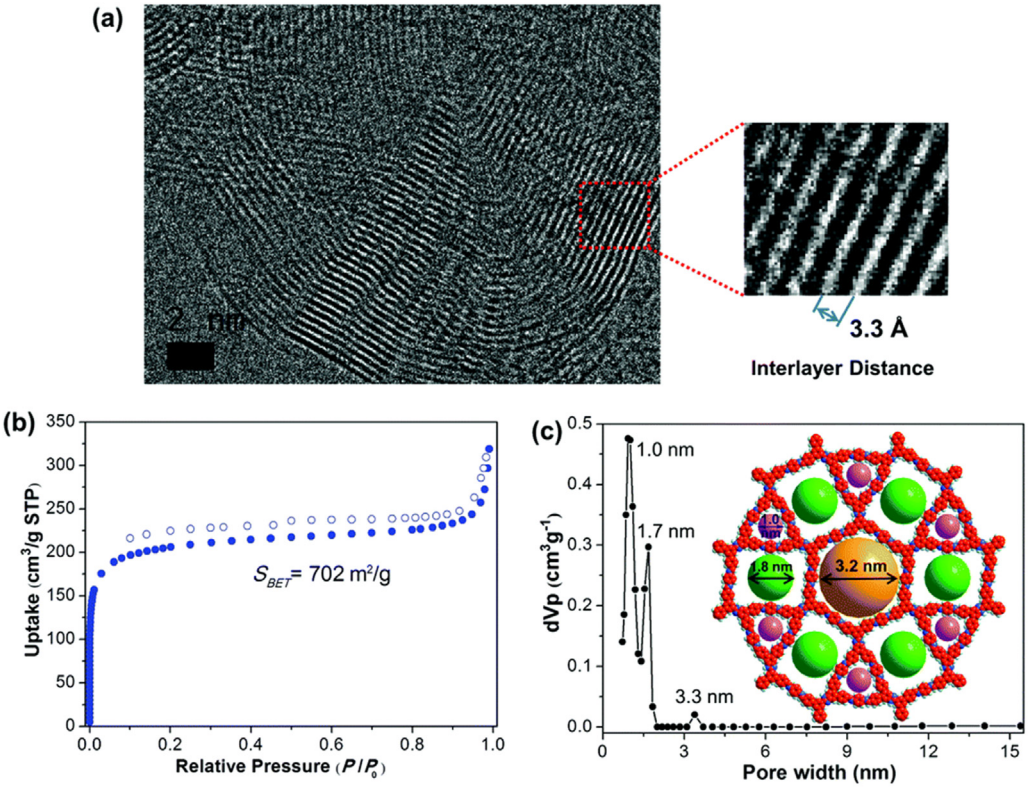

Fig. 29

(a) TEM image of 2D BITA–PDA COF displaying the interlayer packing structure, (b) N_2 adsorption/desorption isotherms at 77 K, and (c) the corresponding pore size distribution result. (Adapted from Ref. [147] with permission; copyright 2017, Royal Society of Chemistry).

Data availability

No data was used for the research described in the article.

Supplementary materials

Supplementary material associated with this article can be found, in the online version, at doi:10.1016/j.giant.2023.100170.

References

[1] K.S. Novoselov, A.K. Geim, S.V. Morozov, D. Jiang, M.I. Katsnelson, I.V. Grigorieva, S.V. Dubonos, A.A. Firsov, Two-dimensional gas of massless Dirac fermions in graphene, Nature 438 (2005) 197–200.

[2] P. Miro, M. Audiffred, T. Heine, An atlas of two-dimensional materials, Chem. Soc. Rev. 43 (2014) 6537–6554.

[3] C. Liu, J. Wang, J. Wan, C. Yu, MOF-on-MOF hybrids: Synthesis and applications, Coord. Chem. Rev. 432 (2021) 213743.

[4] J. Tang, Y. Yamauchi, MOF morphologies control, Nature Chem. 8 (2016) 638–639.

[5] Z. Zheng, H.L. Nguyen, N. Hanikel, K.K.Y. Li, Z. Zhou, T. Ma, O.M. Yaghi, High-yield, green and scalable methods for producing MOF-303 for water harvesting from desert air, Nature Protocols 18 (2023) 136–156.

[6] A.P. Cote, A.I. Benin, N.W. Ockwig, M. O'Keeffe, A.J. Matzger, O.M. Yaghi, Porous, crystalline, covalent organic frameworks, Science 310 (2005) 1166–1170.

[7] P.J. Waller, F. Gandara, O.M. Yaghi, Chemistry of covalent organic frameworks, Acc. Chem. Res. 48 (2015) 3053–3063.

[8] W.W. Zhang, L.J. Chen, S. Dai, C.X. Zhao, C. Ma, L. Wei, M.H. Zhu, S.Y. Chong, H.F. Yang, L.J. Liu, Y. Bai, M.J. Yu, Y.J. Xu, X.W. Zhu, Q. Zhu, S.H. An, R.S. Sprick, M.A. Little, X.F. Wu, S. Jiang, Y.Z. Wu, Y.B. Zhang, H. Tian, W.H. Zhu, A.I. Cooper, Reconstructed covalent organic frameworks, Nature 604 (2022) 72–79.

[9] N. Keller, T. Bein, Optoelectronic processes in covalent organic frameworks, Chem. Soc. Rev. 50 (2021) 1813–1845.

[10] M. Lu, M. Zhang, J. Liu, Y.F. Chen, J.P. Liao, M.Y. Yang, Y.P. Cai, S.L. Li, Y.Q. Lan, Covalent organic framework based functional materials: important catalysts for efficient CO_2 utilization, Angew. Chem. Int. Ed. 61 (2022) e202200003.

[11] S. Manzeli, D. Ovchinnikov, D. Pasquier, O.V. Yazyev, A. Kis, 2D transition metal dichalcogenides, Nature Rev. Mater. 2 (2017) 17033.

[12] R. Lv, J.A. Robinson, R.E. Schaak, D. Sun, Y. Sun, T.E. Mallouk, M. Terrones, Transition metal dichalcogenides and beyond: synthesis, properties, and applications of single and few-layer nanosheets, Acc. Chem. Res. 48 (2015) 56–64.

[13] P. Ranjan, J.M. Lee, P. Kumar, A. Vinu, Borophene: new sensation in flatland, Adv. Mater. 32 (2020) 2000531.

[14] X. Liu, Q. Li, Q. Ruan, M.S. Rahn, B.I. Yakobson, M.C. Hersam, Borophene synthesis beyond the single-atomic-layer limit, Nature Mater. 21 (2022) 35–40.

[15] Z. Dai, L. Liu, Z. Zhang, Strain engineering of 2D materials: issues and opportunities at the interface, Adv. Mater. 31 (2019) 1805417.

[16] F.C. de Lima, G.J. Ferreira, R.H. Miwa, Topological flat band, Dirac fermions and quantum spin Hall phase in 2D Archimedean lattices, Phys. Chem. Chem. Phys. 21 (2019) 22344–22350.

[17] L. Kormos, P. Prochazka, A.O. Makoveev, J. Cechal, Complex k-uniform tilings by a simple bitopic precursor self-assembled on Ag(001) surface, Nature Commun. 11 (2020) 1856.

[18] M.I. Clerc, A. Jagannathan, P. Kalugin, J.F. Sadoc, Square-triangle tilings: an infinite playground for soft matter, Soft Matter. 17 (2021) 6560–9575.

[19] A. Takano, W. Kawashima, A. Noro, Y. Isono, N. Tanaka, T. Dotera, Y. Matsushita, A mesoscopic archimedean tiling having a new complexity in an ABC star polymer, J. Polym. Sci. Part B Polym. Phys. 43 (2005) 2427–2432.

[20] Y. Matsushita, A. Takano, K. Hayashida, T. Asari, A. Noro, Hierarchical nanophase-separated structures created by precisely-designed polymers with complexity, Polymer 50 (2009) 2191–2203.

[21] Y. Matsushita, Precise molecular design of complex polymers and morphology control of their hierarchical multiphase structures, Polym. J. 40 (2008) 177–183.

[22] Y. Matsushita, Creation of hierarchically ordered nanophase structures in block polymers having various competing interactions, Macromolecules 40 (2007) 771–776.

[23] Y. Matsushita, K. Hayashida, T. Dotera, A. Takano, Kaleidoscopic morphologies from ABC star-shaped terpolymers, J. Phys. Condens. Matter 23 (2011) 284111.

[24] K. Ueda, T. Dotera, T. Gemma, Photonic band structure calculations of two-dimensional Archimedean tiling patterns, Phys. Rev. B 75 (2007) 195122.

[25] J.A. Millan, D. Ortiz, G. van Adners, S.C. Glotzer, Self-assembly of archimedean

tilings with enthalpically and entropically patchy polygons, ACS Nano 8 (2014) 2918–2928.

[26] C. Janot, Quasicrystals-A Primer, Oxford University Press, New York, 1994.

[27] T. Dotera, Quasicrystals in soft matter, Israel J. Chem. 51 (2011) 1197–1205.

[28] S.W. Kuo, Hydrogen bonding mediated self-assembled structures from block copolymer mixtures to mesoporous materials, Polym. Inter. 71 (2022) 393–410.

[29] M.G. Mohamed, E.C. Atayde, B.M. Matsagar, J. Na, Y. Yamauchi, K.C.W. Wu, S.W. Kuo, Construction hierarchically mesoporous/microporous materials based on block copolymer and covalent organic framework, J. Taiwan Inst. Chem. Eng. 112 (2020) 180–192.

[30] C. Tscherske, Liquid crystal engineering – new complex mesophase structures and their relations to polymer morphologies, nanoscale patterning and crystal engineering, Chem. Soc. Rev. 36 (2007) 1930–1970.

[31] Z. Su, R. Zhang, X.Y. Yan, Q.Y. Guo, J. Huang, W. Shan, Y. Liu, T. Liu, M. Huang, S.Z.D. Cheng, The role of architectural engineering in macromolecular self-assemblies via non-covalent interactions: a molecular LEGO approach, Prog. Polym. Sci. 103 (2020) 101230.

[32] Y. Wang, J. Huang, X.Y. Yan, H. Lei, X.Y. Liu, Q.Y. Guo, Y. Liu, T. Liu, M. Huang, F. Bian, Z. Su, S.Z.D. Cheng, Soft alloys constructed with distinct mesoatoms via self-sorting assembly of giant shape amphiphiles, Angew. Chem. Int. Ed. 61 (2022) e202200637.

[33] Y. Liu, T. Liu, X. yun Yan, Q.-Y.Y. Guo, J. Wang, R. Zhang, S. Zhang, Z. Su, J. Huang, G.-X.X. Liu, W. Zhang, W. Zhang, T. Aida, K. Yue, M. Huang, S.Z.D. Cheng, A.C. Shi, Mesoatom alloys via self-sorting approach of giant molecules blends, Giant 4 (2020) 100031.

[34] X.-Y. Yan, Q.-Y. Guo, X.-Y. Liu, Y. Wang, J. Wang, Z. Su, J. Huang, F. Bian, H. Lin, M. Huang, Z. Lin, T. Liu, Y. Liu, S.Z.D. Cheng, Superlattice engineering with chemically precise molecular building blocks, J. Am. Chem. Soc. 143 (2021) 21613–21621.

[35] H. Lei, Y. Liu, T. Liu, Q. Guo, X. Yan, Y. Wang, W. Zhang, Z. Su, J. Huang, W. Xu, F. Bian, M. Huang, S.Z.D. Cheng, Unimolecular nanoparticles toward more precise regulations of self-assembled superlattices in soft matter, Angew. Chemie Int. Ed. 61 (2022) e202203433.

[36] R.R. Liang, S.Y. Jiang, R. Han, X. Zhao, Two-dimensional covalent organic frameworks with hierarchical porosity, Chem. Soc. Rev. 49 (2020) 3920–3951.

[37] S.W. Kuo, Hydrogen Bonding in Polymeric Materials, John Wiley & Sons, 2018.

[38] G.M. Grason, B.A. DiDonna, R.D. Kamien, Geometric theory of diblock copolymer phases, Phys. Rev. Lett. 91 (2003) 058304.

[39] S.W. Kuo, Hydrogen bond-mediated self-assembly and supramolecular structures of diblock copolymer mixtures, Polym. Inter. 58 (2009) 455–464.

[40] C.A. Tyler, J. Qin, F.S. Bates, D.C. Morse, SCFT study of nonfrustrated ABC triblock copolymer melts, Macromolecules 40 (2007) 4654–4668.

[41] W. Zheng, Z.G. Wang, Morphology of ABC triblock copolymers, Macromolecules 28 (1995) 7215–7223.

[42] Y. Matsushita, K. Hayashida, A. Takano, Jewelry box of morphologies with mesoscopic length scales – ABC star-shaped terpolymers, Macromol. Rapid Commun. 31 (2010) 1579–1587.

[43] K. Hayashida, A. Takano, S. Arai, Y. Shinohara, Y. Amemiya, Y. Matsushita, Systematic transitions of tiling patterns formed by ABc star-shaped terpolymers, Macromolecules 39 (2006) 9402–9408.

[44] K. Hayashida, W. Kawashima, A. Takano, Y. Shinohara, Y. Amemiya, Y. Nozue, M. Matsushita, Archimedean Tiling Patterns of ABC Star-Shaped Terpolymers Studied by Microbeam Small-Angle X-ray Scattering, Macromolecules 39 (2006) 4869–4872.

[45] J. Park, S. Jang, J.K. Kim, Morphology and microphase separation of star copolymers, J. Polym. Sci. Part B Polym. Phys. 53 (2015) 1–21.

[46] M. Qian, Y. Xu, Formation of perpendicular three-dimensional network nanostructures in ABC-star copolymers, Langmuir 38 (2022) 7889–7897.

[47] H. Huckstadt, A. Gopfert, V. Abtez, Synthesis and morphology of ABC heteroarm star terpolymers of polystyrene, polybutadiene and poly(2-vinylpyridine), Macromol. Chem. Phys. 201 (2000) 296–307.

[48] Y. Matsushita, A. Takano, M. Vayer, C. Sinturel, Nonclassical block copolymer self-assembly resulting from a constrained location of chains and junctions, Adv. Mater. Interface 7 (2020) 1902007.

[49] S.H. Han, V. Pryamitsyn, D. Bae, J. Kwak, V. Ganesan, J.K. Kim, Highly asymmetric lamellar nanopatterns via block copolymer blends capable of hydrogen bonding, ACS Nano 6 (2012) 7966–7972.

[50] J.Q. Zhao, E.M. Pearce, T.K. Kwei, Binary and ternary blends of polystyrene-block-poly(p-hydroxystyrene), Macromolecules 30 (1997) 7119–7126.

[51] K. Dobrosielska, S. Wakao, A. Takano, Y. Matsushita, Nanophase-separated structures of ab block copolymer/c homopolymer blends with complementary hydrogen-bonding interactions, Macromolecules 41 (2008) 7695–7698.

[52] K. Dobrosielska, S. Wakao, J. Suzuki, K. Noda, A. Takano, Y. Matsushita, Effect of homopolymer molecular weight on nanophase-separated structures of AB block copolymer/c homopolymer blends with hydrogen-bonding interactions, Macromolecules 42 (2009) 7098–7102.

[53] S.C. Chen, S.W. Kuo, U.S. Jeng, C.J. Su, F.C. Chang, On modulating the phase behavior of block copolymer/homopolymer blends via hydrogen bonding, Macromolecules 43 (2010) 1083–1092.

[54] S.C. Tsai, Y.C. Lin, E.L. Lin, Y.W. Chiang, S.W. Kuo, Hydrogen bonding strength effect on self-assembly supramolecular structures of diblock copolymer/homopolymer blends, Polym. Chem. 7 (2016) 2395–2409.

[55] W.C. Chen, S.W. Kuo, U.S. Jeng, F.C. Chang, Self-assembly through competitive interactions of miscible diblock copolymer/homopolymer blends: poly(vinylphenol-b-methyl methacrylate)/poly(vinylpyrrolidone) blend, Macromolecules 41 (2008) 1401–1410.

[56] W.C. Chen, S.W. Kuo, C.H. Lu, U.S. Jeng, F.C. Chang, Self-assembly structures through competitive interactions of crystalline−amorphous diblock copolymer/homopolymer blends: poly(ε-caprolactone-b-4-vinyl pyridine)/poly(vinyl phenol), Macromolecules 42 (2009) 3580–3590.

[57] A. Dehghan, A.C. Shi, Modeling hydrogen bonding in diblock copolymer/homopolymer blends, Macromolecules 46 (2013) 5796–5805.

[58] W.C. Su, F.C. Tsai, C.F. Huang, L. Dai, S.W. Kuo, Flexible epoxy resins formed by blending with the diblock copolymer PEO-b-PCL and using a hydrogen-bonding benzoxazine as the curing agent, Polymers 11 (2019) 201.

[59] T. Asari, S. Matsuo, A. Takano, Y. Matsushita, Three-phase hierarchical structures from AB/CD diblock copolymer blends with complemental hydrogen bonding interaction, Macromolecules 38 (2005) 8811–8815.

[60] W.C. Chen, S.W. Kuo, F.C. Chang, Self-assembly of an A–B diblock copolymer blended with a C homopolymer and a C–D diblock copolymer through hydrogen bonding interaction, Polymer 51 (2010) 4176–4184.

[61] T.C. Tseng, S.W. Kuo, Hydrogen-bonding strength influences hierarchical self-assembled structures in unusual miscible/immiscible diblock copolymer blends, Macromolecules 51 (2018) 6451–6459.

[62] T.C. Tseng, S.W. Kuo, Hierarchical self-assembled structures from diblock copolymer mixtures by competitive hydrogen bonding strength, Molecules 23 (2018) 2242.

[63] T.C. Tseng, S.W. Kuo, Hydrogen bonding induces unusual self-assembled structures from mixtures of two miscible disordered diblock copolymers, Eur. Polym. J. 116 (2019) 361–369.

[64] C.T. Tsou, S.W. Kuo, Competing hydrogen bonding interaction creates hierarchically ordered self-assembled structures of PMMA-b-P4VP/PVPh-b-PS mixtures, Macromolecules 52 (2019) 8374–8383.

[65] S. Jiang, A. Gopfert, V. Abetz, Novel morphologies of block copolymer blends via hydrogen bonding, Macromolecules 36 (2003) 6171–6177.

[66] T. Asari, S. Arai, A. Takano, Y. Matsushita, Archimedean tiling structures from ABA/CD block copolymer blends having intermolecular association with hydrogen bonding, Macromolecules 39 (2006) 2232–2237.

[67] H. Miyase, Y. Asai, A. Takano, Y. Matsushita, Kaleidoscopic tiling patterns with large unit cells from ABC star-shaped terpolymer/diblock copolymer blends with hydrogen bonding interaction, Macromolecules 50 (2017) 979–986.

[68] Z.C. Xie, T.H. Gao, X.T. Guo, Q. Xie, Influence of the isothermal process at glass transition temperature on growths of Frank–Kasper polyhedral clusters in TiAl3 alloy, J. Non. Cryst. Solids 406 (2014) 95–101.

[69] S. Lee, M.J. Bluemle, F.S. Bates, Discovery of a Frank-Kasper σ phase in sphere-forming block copolymer melts, Science 330 (2010) 349–353.

[70] B.K. Cho, A. Jian, S.M. Gruner, U. Wiesner, Mesophase structure-mechanical and ionic transport correlations in extended amphiphilic dendrons, Science 305 (2004) 1598–1601.

[71] H.J. Sun, S. Zhang, V. Perece, From structure to function via complex supramolecular dendrimer systems, Chem. Soc. Rev. 44 (2015) 3900–3923.

[72] G. Ungar, X. Zeng, Frank–Kasper, quasicrystalline and related phases in liquid crystals, Soft Matter 1 (2005) 95–106.

[73] X.H. Cheng, S. Diele, C. Tschierske, Molecular design of liquid-crystalline block molecules: semifluorinated pentaerythritol tetrabenzoates exhibiting lamellar, columnar, and cubic mesophases, Angew Chem. Int. Ed. 39 (2000) 592–595.

[74] M. Huang, K. Yue, J. Wang, C.H. Hsu, L. Wang, S.Z.D. Cheng, Frank-Kasper and related quasicrystal spherical phases in macromolecules, Sci. China Chem. 61 (2018) 33–45.

[75] S. Lee, C. Leighton, F.S. Bates, Sphericity and symmetry breaking in the formation of Frank–Kasper phases from one component materials, Proc. Natl. Acad. Sci 111 (2014) 17723–17731.

[76] K.K. Lachmayr, L.R. Sita, Small-molecule modulation of soft-matter Frank–Kasper phases: a method for adding function to form, Angew. Chem. Int. Ed. 59 (2020) 3563–3567.

[77] B. Nouri, C.Y. Chen, J.M. Lin, H.L. Chen, Phase control of colloid-like block copolymer micelles by tuning size distribution via thermal processing, Macromolecules 55 (2022) 9820–9832.

[78] M.Z. Chen, Y.T. Huang, C.Y. Chen, H.L. Chen, Accessing the Frank−Kasper σ phase of block copolymer with small conformational asymmetry via selective solvent solubilization in the micellar corona, Macromolecules 55 (2022) 10812–10820.

[79] K. Chen, C.Y. Chen, H.L. Chen, R. Komaki, N. Kawakami, T. Isono, T. Satoh, D.Y. Hung, Y.L. Liu, Self-assembly behavior of sugar-based block copolymers

in the complex phase window modulated by molecular architecture and configuration, Macromolecules 56 (2023) 28–39.

[80] W.C. Chen, Y.Z. Liu, S.W. Kuo, Mesoporous organic/inorganic hybrid materials with Frank-Kasper phases templated by an unusual linear symmetry diblock copolymer, Macromol. Rapid Commun. 42 (2021) 2100302.

[81] Y. Miyamori, J. Suzuki, A. Takano, Y. Matsushita, Periodic and aperiodic tiling patterns from a tetrablock terpolymer system of the A1BA2C type, ACS Macro Lett. 9 (2020) 32–37.

[82] M. Suzuki, T. Orido, A. Takano, Y. Matsushita, The largest quasicrystalline tiling with dodecagonal symmetry from a single pentablock quarterpolymer of the AB1CB2D Type, ACS Nano 16 (2022) 6111–6117.

[83] K. Aissou, W. Kwon, M. Mumtaz, S. Antoine, M. Maret, G. Portale, G. Fleury, G. Hadziioannou, Archimedean Tilings and hierarchical lamellar morphology formed by semicrystalline Miktoarm star terpolymer thin films, ACS Nano 10 (2016) 4055–4061.

[84] M. Watanable, Y. Asai, J. Suzuki, A. Takano, Y. Matsushita, Frank-Kasper A15 phase formed in ABn block-graft copolymers with large numbers of graft chains, Macromolecules 53 (2020) 10217–10224.

[85] M.W. Bates, J. Lequieu, S.M. Barbon, R.M. Lewis III, K.T. Delaney, A. Anastasaki, C.J. Hawker, G.H. Fredrickson, C.M. Bates, Stability of the A15 phase in diblock copolymer melts, Proc. Natl. Acad. Sci. 116 (2019) 13194–13199.

[86] S. Jeon, T. Jun, S. Jo, H. Ahn, S. Lee, B. Lee, D.Y. Ryu, Frank–Kasper phases identified in PDMS-b-PTFEA copolymers with high conformational asymmetry, Macromol. Rapid Commun. 40 (2019) 1900259.

[87] B. Nouri, Y.C. Chen, Y.S. Huang, B.W. Mansel, H.L. Chen, Emergence of a metastable laves C14 phase of block copolymer micelle bearing a glassy core, Macromolecules 54 (2021) 9195–9203.

[88] A.J. Mueller, A.P. Lindsay, A. Jayaraman, T.P. Lodge, M.K. Mahanthappa, F.S. Bates, Emergence of a C15 laves phase in diblock polymer/homopolymer blends, ACS Macro Lett. 9 (2020) 576–582.

[89] A.F.M. EL-Mahdy, T.C. Yu, M.G. Mohamed, S.W. Kuo, Secondary structures of polypeptide-based diblock copolymers influence the microphase separation of templates for the fabrication of microporous carbons, Macromolecules 54 (2021) 1030–1042.

[90] A.F.M. EL-Mahdy, T.E. Liu, S.W. Kuo, Direct synthesis of nitrogen-doped mesoporous carbons from triazine-functionalized resol for CO2 uptake and highly efficient removal of dyes, J. Hazard. Mater. 391 (2020) 122163.

[91] A.F.M. EL-Mahdy, T.C. Yu, S.W. Kuo, Synthesis of multiple heteroatom–doped mesoporous carbon/silica composites for supercapacitors, Chem. Eng. J. 414 (2021) 128796.

[92] S.W. Kuo, Hydrogen bonding interactions in polymer/polyhedral oligomeric silsesquioxane nanomaterials, J. Polym. Res. 29 (2022) 69.

[93] M.G. Mohamed, S.W. Kuo, Progress in the self-assembly of organic/inorganic polyhedral oligomeric silsesquioxane (POSS) hybrids, Soft Matter. 18 (2022) 5535–5561.

[94] C. Xiao, N. Fujita, K. Miyasaka, Y. Sakamoto, O. Teraski, Dodecagonal tiling in mesoporous silica, Nature 487 (2012) 349–353.

[95] Y.C. Huang, W.C. Chen, S.W. Kuo, Mesoporous phenolic/POSS hybrids induced by microphase separation arising from competitive hydrogen bonding interactions, Macromolecules 55 (2022) 8918–8930.

[96] M. Huang, C.H. Hsu, J. Wang, S. Mei, X. Dong, Y. Li, M. Li, H. Liu, W. Zhang, T. Aida, W.B. Zhang, K. Yue, S.Z.D. Cheng, Selective assemblies of gianttetrahedra via precisely controlled positional interactions, Science 348 (2015) 424–428.

[97] Z. Su, C.H. Hsu, Z. Gong, X. Feng, J. Huang, R. Zhang, Y. Wang, J. Mao, C. Wesdemiotis, T. Li, S. Seifert, W. Zhang, T. Aida, M. Huang, S.Z.D. Cheng, Identification of a Frank–Kasper Z phase from shape amphiphile self-assembly, Nature Chem. 11 (2019) 899–905.

[98] X. Feng, G. Liu, D. Guo, K. Lang, R. Zhang, J. Huang, Z. Su, Y. Li, M. Huang, T. Li, S.Z.D. Cheng, Transition kinetics of self-assembled supramolecular dodecagonal quasicrystal and Frank–Kasper σ phases in ABn Dendron-like giant molecules, ACS Macro Lett. 8 (2019) 875–881.

[99] Y. Liu, T. Liu, X.Y. Yan, Q.Y. Guo, H. Lei, Z. Huang, R. Zhang, Y. Wang, J. Wang, F. Liu, F.G. Bian, E.W. Meijer, T. Aida, M. Huang, S.Z.D. Cheng, Expanding quasiperiodicity in soft matter: supramolecular decagonal quasicrystals by binary giant molecule blends, Proc. Natl. Acad. Sci. 119 (2022) e2115304119.

[100] K. Yue, M. Huang, R.L. Marson, J. He, J. Huang, Z. Zhou, J. Wang, C. Liu, X. Yan, K. Wu, Z. Guo, H. Liu, W. Zhang, P. Ni, C. Wesdemiotis, W.B. Zhang, S.C. Glotzer, S.Z.D. Cheng, Geometry induced sequence of nanoscale Frank–Kasper and quasicrystal mesophases in giant surfactants, Proc. Natl. Acad. Sci. 113 (2016) 14195–14200.

[101] H.M. El-Kaderi, J.R. Hunt, J.L. Mendoza-Cortés, A.P. Côté, R.E. Taylor, M. O'Keeffe, O.M. Yaghi, Designed synthesis of 3D covalent organic frameworks, Science 316 (2007) 268–272.

[102] C.S. Diercks, O.M. Yaghi, The atom, the molecule, and the covalent organic framework, Science 355 (2017) 1585.

[103] R.K. Sharma, P. Yadav, M. Yadav, R. Gupta, P. Rana, A. Srivastava, R. Zbořil, R.S. Varma, M. Antonietti, M.B. Gawande, Recent development of covalent organic frameworks (COFs): synthesis and catalytic (organic-electro-photo) applications, Mater. Horizons 7 (2020) 411–454.

[104] N. Huang, P. Wang, D. Jiang, Covalent organic frameworks: a materials platform for structural and functional designs, Nat. Rev. Mater. 1 (2016) 1–19.

[105] A.F.M. El-Mahdy, Y.H. Hung, T.H. Mansoure, H.H. Yu, T. Chen, S.W. Kuo, A hollow microtubular triazine-and benzobisoxazole-based covalent organic framework presenting sponge-like shells that functions as a high-performance supercapacitor, Chem. Asian J. 14 (2019) 1429–1435.

[106] A.F.M. EL-Mahdy, C. Young, J. Kim, J. You, Y. Yamauchi, S.W. Kuo, Hollow microspherical and microtubular [3+3] carbazole-based covalent organic frameworks and their gas and energy storage applications, ACS Appl. Mater. Interfaces 11 (2019) 9343–9354.

[107] M.S. Lohse, T. Bein, Covalent organic frameworks: structures, synthesis, and applications, Adv. Funct. Mater. 28 (2018) 1705553.

[108] W.T. Chung, I.M.A. Mekhemer, M.G. Mohamed, A.M. Elewa, A.F.M. EL-Mahdy, H.H. Chou, S.W. Kuo, K.C.W. Wu, Recent advances in metal/covalent organic frameworks based materials: their synthesis, structure design and potential applications for hydrogen production, Coord. Chem. Rev. 483 (2023) 215066.

[109] M. Gao, M.J. Zheng, A.F.M. EL-Mahdy, C.W. Chang, Y.C. Su, W.H. Hung, S.W. Kuo, L.H. Yeh, A bioinspired ionic diode membrane based on sub-2 nm covalent organic framework channels for ultrahigh osmotic energy generation, Nano Energy 105 (2023) 108007.

[110] H.R. Abuzeid, A.F.M. EL-Mahdy, S.W. Kuo, Covalent organic frameworks: Design principles, synthetic strategies, and diverse applications, Giant 6 (2021) 100054.

[111] M.G. Mohamed, M.H. Elsayed, Y. Ye, M.M. Samy, A.E. Hassan, T.H. Mansoure, Z. Wen, H.H. Chou, K.H. Chen, S.W. Kuo, Construction of porous organic/inorganic hybrid polymers based on polyhedral oligomeric silsesquioxane for energy storage and hydrogen production from water, Polymers 15 (2023) 182.

[112] M. Ejaz, M.M. Samy, Y. Ye, S.W. Kuo, M.G. Mohamed, Design hybrid porous organic/inorganic polymers containing polyhedral oligomeric silsesquioxane/pyrene/anthracene moieties as a high-performance electrode for supercapacitor, Int. J. Molecular Sci. 24 (2023) 2501.

[113] M.M. Samy, M.G. Mohamed, S.U. Sharma, S.V. Chaganti, T.H. Mansoure, J.T. Lee, T. Chen, S.W. Kuo, Constructing conjugated microporous polymers containing triphenylamine moieties for high-performance capacitive energy storage, Polymer 264 (2023) 125541.

[114] Y. Xu, S. Jin, H. Xu, A. Nagai, D. Jiang, Conjugated microporous polymers: design, synthesis and application, Chem. Soc. Rev. 42 (2013) 8012–8031.

[115] A.I. Copper, Conjugated microporous polymers, Adv. Mater. 26 (2009) 1291–1295.

[116] M.G. Mohamed, A.F.M. EL-Mahdy, M.G. Kotp, S.W. Kuo, Advances in porous organic polymers: syntheses, structures, and diverse applications, Mater. Adv. 3 (2022) 707–733.

[117] M.M. Samy, I.M.A. Mekhemer, M.G. Mohamed, M.H. Elsayed, K.H. Lin, Y.K. Chen, T.L. Wu, H.H. Chou, S.W. Kuo, Conjugated microporous polymers incorporating Thiazolo[5,4-d]thiazole moieties for Sunlight-Driven hydrogen production from water, Chem. Eng. J. 446 (2022) 137158.

[118] Y. Sheng, Q. Chen, S.M. Mahurin, R.T. Mayes, W. Zhan, J. Zhang, H. Liu, S. Dai, Fibers with hyper-crosslinked functional porous frameworks, Macromol. Rapid Commun. 39 (2018) 1700767.

[119] M.G. Mohamed, M.M.M. Ahmed, W.T. Du, S.W. Kuo, Meso/microporous carbons from conjugated hyper-crosslinked polymers based on tetraphenylethene for high-performance CO_2 capture and supercapacitor, Molecules 26 (2021) 738.

[120] M.G. Mohamed, M.Y. Tsai, C.F. Wang, C.F. Huang, M. Danko, L. Dai, T. Chen, S.W. Kuo, Multifunctional polyhedral oligomeric silsesquioxane (POSS) Based hybrid porous materials for CO_2 uptake and iodine adsorption, Polymers 13 (2021) 221.

[121] M.G. Mohamed, S.U. Sharma, N.Y. Liu, T.H. Mansoure, M.M. Samy, S.V. Chaganti, Y.L. Chang, J.T. Lee, S.W. Kuo, Ultrastable covalent triazine organic framework based on anthracene moiety as platform for high-performance carbon dioxide adsorption and supercapacitors, Int. J. Mol. Sci. 23 (2022) 3174.

[122] M. Liu, L. Guo, S. Jin, B. Tan, Covalent triazine frameworks: synthesis and applications, J. Mater. Chem. A 7 (2019) 5153–5172.

[123] L. Liao, M. Li, Y. Yin, J. Chen, Q. Zhong, R. Du, S. Liu, Y. He, W. Fu, F. Zeng, ACS Omega 8 (2023) 4527–4542.

[124] A.F.M. EL-Mahdy, Y.H. Hung, T.H. Mansoure, H.H. Yu, Y.S. Hsu, K.C.W. Wu, S.W. Kuo, Synthesis of [3+3] β-ketoenamine-tethered covalent organic frameworks (COFs) for high-performance supercapacitance and CO_2 storage, J. Taiwan Inst. Chem. Eng. 103 (2019) 199–208.

[125] C.R. Deblase, K.E. Silberstein, T.T. Truong, H.D. Abruña, R W, Dichtel, β-ketoenamine-linked covalent organic frameworks capable of pseudocapacitive energy storage, J. Am. Chem. Soc. 135 (2013) 16821–16824.

[126] L. Liu, W.K. Meng, Y.S. Zhou, X. Wang, G.J. Xu, M.L. Wang, J.M. Lin, R.S. Zhao, β-Ketoenamine-linked covalent organic framework coating for ultra-high-performance solid-phase microextraction of polybrominated diphenyl ethers from environmental samples, Chem. Eng. J. 356 (2019) 926–933.

[127] H.R. Abuzeid, A.F.M. El-Mahdy, M.M.M. Ahmed, S.W. Kuo,

Triazine-functionalized covalent benzoxazine framework for direct synthesis of N-doped microporous carbon, Polym. Chem. 10 (2019) 6010–6020.

[128] Q. Fang, Z. Zhuang, S. Gu, R.B. Kaspar, J. Zheng, J. Wang, S. Qiu, Y. Yan, Designed synthesis of large-pore crystalline polyimide covalent organic frameworks, Nat. Commun. 5 (2014) 4503.

[129] Y. Zhang, Z. Huang, B. Ruan, X. Zhang, T. Jiang, N. Ma, F.C. Tsai, Design and synthesis of polyimide covalent organic frameworks, Macromol. Rapid Commun. 41 (2020) 200402.

[130] A.F.M. El-Mahdy, C.H. Kuo, A. Alshehri, C. Young, Y. Yamauchi, J. Kim, S.W. Kuo, Strategic design of triphenylamine- and triphenyltriazine-based two-dimensional covalent organic frameworks for CO2 uptake and energy storage, J. Mater. Chem. A 6 (2018) 19532–19541.

[131] M.G. Mohamed, C.C. Lee, A.F.M. EL-Mahdy, J. Lüder, M.H. Yu, Z. Li, Z. Zhu, C.C. Chueh, S.W. Kuo, Exploitation of two-dimensional conjugated covalent organic frameworks based on tetraphenylethylene with bicarbazole and pyrene units and applications in perovskite solar cells, J. Mater. Chem. A 8 (2020) 11448–11459.

[132] A.F.M. EL-Mahdy, M.B. Zakaria, H.X. Wang, T. Chen, Y. Yamauchi, S.W. Kuo, Heteroporous bifluorenylidene-based covalent organic frameworks displaying exceptional dye adsorption behavior and high energy storage, J. Mater. Chem. A 8 (2020) 25148–25155.

[133] A.F.M. EL-Mahdy, A.M. Elewa, S. Huang, H. Chou, S.W. Kuo, Dual-function fluorescent covalent organic frameworks: HCl sensing and photocatalytic H_2 evolution from water, Adv. Opt. Mater. 8 (2020) 2000641.

[134] A.F.M. El-Mahdy, M.G. Mohamed, T.H. Mansoure, H.H. Yu, T. Chen, S.W. Kuo, Ultrastable tetraphenyl-p-phenylenediamine-based covalent organic frameworks as platforms for high-performance electrochemical supercapacitors, Chem. Commun. 55 (2019) 14890–14893.

[135] S. Dalapati, M. Addicoat, S. Jin, T. Sakurai, J. Gao, H. Xu, S. Irle, S. Seki, D. Jiang, Rational design of crystalline supermicroporous covalent organic frameworks with triangular topologies, Nature Commun. 6 (2015) 7786.

[136] K. Geng, V. Arumugam, H. Xu, Y. Gao, D. Jiang, Covalent organic frameworks: polymer chemistry and functional design, Prog. Polym. Sci. 108 (2020) 101288.

[137] Z.F. Pang, T.Y. Zhou, R.R. Liang, Q.Y. Qi, X. Zhao, Regulating the topology of 2D covalent organic frameworks by the rational introduction of substituents, Chem. Sci. 8 (2017) 3866–3870.

[138] R.R. Liang, S.Y. Jiang, H.A R, X. Zhao, Two-dimensional covalent organic frameworks with hierarchical porosity, Chem. Soc. Rev. 49 (2020) 3920–3951.

[139] Y. Li, W. Chen, G. Xing, D. Jiang, L. Chen, New synthetic strategies toward covalent organic frameworks, Chem. Soc. Rev. 49 (2020) 2852–2868.

[140] T. Sick, A.G. Hufnagel, J. Kampmann, I. Kondofersky, M. Calik, J.M. Rotter, A. Evans, M. Döblinger, S. Herbert, K. Peters, D. Böhm, P. Knochel, D.D. Medina, D.F. Rohlfing, T. Bein, Oriented films of conjugated 2D covalent organic frameworks as photocathodes for water splitting, J. Am. Chem. Soc. 140 (2018) 2085–2092.

[141] M.W. Zhu, S.Q. Xu, X.Z. Wang, Y. Chen, L. Dai, X. Zhao, The construction of fluorescent heteropore covalent organic frameworks and their applications in spectroscopic and visual detection of trinitrophenol with high selectivity and sensitivity, Chem. Commun. 54 (2018) 2308–2311.

[142] H.R. Abuzeid, A.F.M. EL-Mahdy, S.W. Kuo, Hydrogen bonding induces dual porous types with microporous and mesoporous covalent organic frameworks based on bicarbazole units, Microporous. Mesoporous. Mater. 300 (2020) 110151.

[143] X. Wang, X. Han, C. Cheng, X. Kang, Y. Liu, Y. Cui, 2D covalent organic frameworks with CEM topology, J. Am. Chem. Soc. 144 (2022) 7366–7373.

[144] M. O'Keeffe, M.A. Peskov, S.J. Ramsden, O.M. Yaghi, The reticular chemistry structure resource (RCSR) database of, and symbols for crystal nets, Acc. Chem. Res. 41 (2008) 1782–1789.

[145] H. Chen, L. Voigt, M. Kubus, D. Mihrin, S. Mossin, R.W. Larsen, S. Kagnas, S. Piligkos, K.S. Pedersen, Magnetic archimedean tessellations in metal−organic frameworks, J. Am. Chem. Soc. 143 (2021) 14041–14045.

[146] J. Mikhael, J. Roth, L. Helden, C. Bechinger, Archimedean-like tiling on decagonal quasicrystalline surfaces, Nature 454 (2008) 501–504.

[147] S.L. Cai, Z.H. He, X.L. Li, K. Zhang, S.R. Zheng, J. Fan, Y. Liu, W.G. Zhang, An unprecedented 2D covalent organic framework with an htb net topology, Chem. Commun. 55 (2019) 13454.

[148] Y. Ge, W. Zhang, Directed synthesis of isomeric 2D heteropore covalent organic frameworks, Sci. China Chem. 66 (2023) 926–927.

[149] S. Patial, V. Soni, A. Kumar, P. Raizada, T. Ahamad, X.M. Pham, Q.V. Le, V.H. Nguyen, S. Thakur, P. Singh, Rational design, structure properties, and synthesis strategies of dual-pore covalent organic frameworks (COFs) for potent applications: a review, Environ. Res. 218 (2023) 114982.